PARAFERMION EXCITATIONS IN HOLE SYSTEMS IN THE $\nu = \frac{1}{3}$ FILLED FRACTIONAL QUANTUM HALL STATE

A Dissertation

Submitted to the Faculty

of

Purdue University

by

Ian A. Arnold

In Partial Fulfillment of the

Requirements for the Degree

of

Doctor of Philosophy

August 2019

Purdue University

West Lafayette, Indiana

THE PURDUE UNIVERSITY GRADUATE SCHOOL
STATEMENT OF DISSERTATION APPROVAL

Dr. Yuli Lyanda-Geller, Chair

Purdue University Department of Physics and Astronomy

Dr. Ephraim Fischbach

Purdue University Department of Physics and Astronomy

Dr. Andrew Hirsch

Purdue University Department of Physics and Astronomy

Dr. Leonid Rokhinson

Purdue University Department of Physics and Astronomy

Approved by:

Dr. John Finley

Head of the School Graduate Program

ACKNOWLEDGMENTS

I would like to thank my advisor, Professor Lyanda-Geller for his instruction and expertise in the last several years of working on this dissertation. After departing my original pursuit in experimental condensed matter physics, I found myself inspired to work in this field in large part because of his input, leadership, and enthusiasm for the subject. I would also like to acknowledge the invaluable input and patience of Dr. George Simion. His correspondence, collaboration, patience, and generosity throughout this work have been what made this possible to begin with.

I would like to thank my committee, Professors Fischbach, Hirsch, and Rokhinson for their guidance, questions, and time they have devoted to my not always convenient requests over the past years. I would like to especially thank Professor Fischbach for the many helpful conversations over all the years of my work here, some of which were responsible for my perseverance towards this goal even in light of setbacks.

I would like to thank my undergraduate advisor Professor Petta at Princeton, and Professor Csathy for being a wonderful first advisor at Purdue. I would also like to thank Professor Ramdas for his guidance, openness and friendship during my time as his teaching assistant. I would also like to thank some of the friends I've made both at Princeton and at Purdue, with whom many conversations have led me toward new progress in my work, including Bobby, Sean, Chris, Ryan, Chris, Jackie, Ethan, Lorenz, and Justin.

I would like to thank my family, my mother Deborah Campana, and father Mitchell Arnold, whose support, advice, and guidance have always provided me with direction and confidence, even when I felt my own confidence wane. Their own experience as Doctors of their respective fields are the original inspiration for my pursuit of this degree, and their characters and lives have and will always serve as beautiful templates after which I hope to model my own. I also want to thank my West

Lafayette family, the Bells, Drs. Mark and Catherine, as well as David, for their constant loving and thoughtful provision for me. Their welcoming and generosity toward me has made their home my other home, both in function and in spirit, not to mention providing moral support when I found myself most demoralized, and their guidance in my faith has become foundational in how I approach my life and work.

Lastly, and most importantly, I want to thank my wonderful fiancée Maria for her incredible love and support throughout the course of my time in this doctoral program. Her belief in me has almost always exceeded my own, and it is my most sincere hope that the completion of this work will make her proud, not just of my achievement, but also of her own accomplishment in being the single greatest reason I have gotten to this point. Her achievements in her own work and life make me proud to be her partner, and I endeavor to live up to that amazing example for her as well.

TABLE OF CONTENTS

LIST OF FIGURES

Figure Page

ABSTRACT

Arnold, Ian A. PhD, Purdue University, August 2019. Parafermion Excitations in Hole Systems in the $\nu = \frac{1}{3}$ Filled Fractional Quantum Hall State. Major Professor: Yuli Lyanda-Geller.

Non-Abelian excitations, including Majorana fermions, parafermions, and Fibonacci anyons, provide potential new settings for realizations of topological quantum computation operations. Topological quantum systems have the advantage of being protected against some types of entanglement with the surrounding environment, but their elusive nature has inspired many to pursue rare systems in which they may be physically realized. In this work we present a new platform for production of parafermions in the $\nu = \frac{1}{3}$ fractional quantum hall effect regime in a two-dimensional hole gas in a Gallium Arsenide quantum well, where spin transitions in the rich Γ_8 Luttinger ground state can be manipulated by gate-controlled electric fields. When numerical and analytical calculations of many-particle interactions combine with a proximity-induced superconducting pairing potential in this system, the spin transition we observe gives rise to a superconducting gap with an onset of six-fold degenerate ground state which disappears at critical values of the gap parameter Δ_k, the energetic signature associated with parafermion production.

1. INTRODUCTION

In the search for a suitable setting for a universal quantum computer, many condensed matter systems have been considered due to their various properties, Hilbert spaces, and types of realizable quantum operations. Among these, the search for a topologically protected, robust system that is protected from errors due to its distinct nature has been an alluring topic of theoretical and experimental inquiry. A main advantage to such a system is that through braiding operations, or manipulation of quasiparticles through swaps around one another, one may weave a system through several of its various degenerate ground states, but the information pertaining to the particular set of operations that led to the system's final state would be preserved by the nature of the braiding transformations' non-Abelian properties [1–7].

Condensed matter systems have always been a forefront of the search for such novel particles because of the richness of the low-dimensional, many particle liquids that exist at low temperatures in semiconductor heterostructures and quantum wells. The collective excitations of these liquids have been shown to exhibit many phenomena that were at the time of their discovery, hitherto unobserved outside of such cold systems, such as fractionally charged particles, anyons with fractional phases, and many more.

Two famous ground states stand out as the most well-known attempts at describing physically realizable non-Abelian states of matter. One that has been investigated for decades is the anomalous $\nu = \frac{5}{2}$ Fractional Quantum Hall Effect (FQHE) that arises in clean systems where one might expect an ungapped Fermi sea of quasielectrons, as is true in the spin branches of the Lowest Landau Level (LLL); however, in this excited Landau Level, a collective effect leads to the formation of a gapped ground state, theorized by Moore and Read to be a topologically distinct state formed by $p-$wave like pairing of electrons [8–13]. Additional exploration into the $\nu = \frac{12}{5}$ state

revealed a possible parafermion-like ground state that would be a suitable setting for quantum computation, but for the small size of the gap [14].

Somewhat more recently, the Kitaev toy model of a $1D$ chain of quasiparticles suggested that with the proximity effect of a local $p-$wave superconductor to induce a particle pairing in a symmetric spin state, one might realize a paired state between the quasiparticles at the end of the chain with one another to create an effect that is a Majorana-like excitation that is not necessarily capable of universal quantum computation, but was proposed as a setting for stable quantum memory for storage of information [3, 7, 15–20]. The Kitaev toy model required several factors in addition to the $p-$wave superconductor proximity effect, namely, an off-diagonal tunneling amplitude wherein quasielectrons had some finite, non-vanishing cost to tunnel from one site in the chain to another. Kitaev suggests in a footnote in the 2001 paper that perhaps a system might exist in which the requirement for triplet, or $p-$wave superconductor pairing might be relaxed in the presence of spin-orbit interaction. This is fortunate, as the existence of $p-$wave, or triplet, superconductors is very seldom realized experimentally, with perhaps the only example being a Strontium Ruthenate (SRO) superconductor [21]. The significant engineering difficulties along with the relatively low T_c of this superconductor, not to mention the inability of the Majorana pairs to create universal quantum operations have made it a less-than-ideal candidate in the long term. As Kitaev predicted, strong spin-orbit interaction removes the necessity for the $p-$wave superconductivity, but the class of quantum operations on the toy chain in the $s-$wave case with spin-orbit interaction is still limited [22–30]. Another candidate system is the popular topological insulator (TI) system's edges [31, 32], but the inherent instability and degradation of the TI could be a disadvantage for the system's use in engineering applications.

Previous work has also attempted to theoretically realize a $\nu = \frac{2}{3}$ FQHE state in a finite-width quantum well in which transverse magnetic fields can manipulate the spin splitting between electrons in order to manipulate the spin degree of freedom, gaining access to parafermion excitations through addition of a superconducting proximity

effect, but the difficulty of imposing the spin degree of freedom through large in-plane magnetic fields may prove a barrier to experimental realization parafermions with this platform [28, 30, 33–35]. Realization of parafermion-supporting platforms may lead to more complex systems of paired parafermions in which can give rise to Fibonacci anions, which may lead to the possibility of realizing a universal quantum computation platform [36].

The work we present here will demonstrate a new theoretical platform that will support generation of parafermions in the $\nu = \frac{1}{3}$ FQHE regime for a two-dimensional hole liquid in a Gallium Arsenide quantum well, motivated by the work in [28] and [30]. The inherent advantage of using holes for this type of pursuit is that there are spin-like (pseudospin) transitions within the ground state of the single particle hole spectrum that can be used to create a strong spin-orbit-like effect without the need to create strong in-plane magnetic fields. The spin characteristics of hole systems' ground states have given led to observations of ground state transitions that are not available to typical two-dimensional electron systems [37]. For one, observation of the even-denominator $\nu = \frac{1}{2}$ FQHE state appearing in hole systems is likely due to the near-degeneracy of different spin species in the ground state of the hole spectrum in Gallium Arsenide [38–40]. This ground state, theorized to be the two-component "Ψ_{331}" state, requires the presence of multiple species of ground state components, which in holes we attribute to the multiple pseudospin species. The $\nu = \frac{1}{2}$ state is observed in two-dimensional electron systems when either a double-layer quantum well [41] or a wide single quantum well [42] are used, both of which give rise to multiple interacting electron sub-bands.

The ground states of the two-dimensional hole gas may be manipulated using gate-controlled DC electric fields in order to force the system into one or another pseudospin ground states at a given magnetic field, allowing much more fine control of the system's spin degree of freedom, similar to Refs. [30, 43]. Subsequent numerical calculations using physical many-particle Coulomb interaction pseudopotentials in a cylindrical system will then yield the $\nu = \frac{1}{3}$ fractional quantum Hall effect ground

state in a system with a topological spin crossing in the center. In such a system it has been proposed that counterpropagating edge currents within a region in a sample might create parafermions if quasiparticles are allowed to tunnel from one edge current to another, and if a superconducting gap might be introduced via a proximity effect.

In our system we demonstrate copropagating edge currents in the spin-transition region in the center of our sample, where the difference in the currents' velocities give rise to the non-zero superconducting gap parameter in the presence of a pairing potential. This allows us impose an s-wave superconducting proximity effect by relaxing particle number conservation in a certain region and allowing creation and annihilation of Cooper pairs via the effective Hamiltonian provided by the position-space Bogoliubov-de Gennes formalismin order to introduce pairing potentials to the spinful system. After establishing this system through numerical calculations we will demonstrate the main character of the energy spectrum of the system we consider: a gapped superconducting system with a with an onset of six-fold degenerate ground state, wherein the gap closes at a range of critical superconducting parameter Δ_k [17]. We also confirm physically realistic values of all experimental parameters needed to realize this system, which may function as an important building block in the road toward a universal quantum computing platform.

2. THE Γ_8 LUTTINGER HAMILTONIAN IN EXTERNAL MAGNETIC AND ELECTRIC FIELDS

2.1 Single Particle Solutions in a Gallium Arsenide Quantum Well

The description due to Luttinger [44] leads us to the single particle Hamiltonian for quasiholes in the Γ_8 degenerate valence subbands near the center of the Brillouin zone in III-V, II-VI, Si, and Ge bulk semiconductors: [45–47]

$$\hat{H} = \frac{\hbar^2}{2m_0}\Bigg[\left(\gamma_1 + \frac{5}{2}\gamma_2\right)\hat{\mathbf{k}}^2 I - 2\gamma_2\left(\hat{k}_x^2 J_x^2 + \hat{k}_y^2 J_y^2 + \hat{k}_z^2 J_z^2\right) - 4\gamma_3\left(\{\hat{k}_x,\hat{k}_y\}\{J_x,J_y\} + \{\hat{k}_y,\hat{k}_z\}\{J_y,J_z\} + \{\hat{k}_z,\hat{k}_x\}\{J_z,J_x\}\right)\Bigg] + \frac{e\hbar}{m_0 c}\left[\kappa\mathbf{J}\cdot\mathbf{B} + q_0\left(J_x^3 B_x + J_y^3 B_y + J_z^3 B_z\right)\right]. \quad (2.1)$$

In this expression the J_i matrices and their multiples are the spin-$\frac{3}{2}$ angular momentum matrices that account for the 4-fold degeneracy at the $Gamma-$point. The brackets $\{A,B\}$ signify the totally antistymmetric combination: $\{A,B\} = \frac{1}{2}(AB + BA)$. The $\gamma_{1,2,3}$ "Luttinger parameters" are phenomenological and can be experimentally determined, and for numerical calculations, our values are $\gamma_1 = 6.8, \gamma_2 = 2.1, \gamma_3 = 2.9$. κ and q_0 are Zeeman-like coefficients. We assume the $J_i^3 B_i$ effect to be small, and thus eventually take $q_0 \approx 0$, while we set $\kappa = 1.2$. These parameters are all typical for GaAs, and have been measured frequently in the literature via measurements of heavy and light hole effective masses.

We consider a two-dimensional hole gas (2DHG) at low temperature in a GaAs quantum well, and we initially assume no confinement in the $x-$ and $y-$directions, the plane of the 2DHG, and a very narrow confinement in the $z-$direction of approximately $2w = 200\mathring{A}$ (for the purposes of numerical calculations). We assume an externally applied magnetic field $\mathbf{B} = -B\hat{z}$ for which we choose the vector potential

$\mathbf{A}$ to be in the Landau gauge $\mathbf{A} = \langle 0, -Bx, 0\rangle$. The quasi-momentum $\hat{k}_\alpha$ operators are given in terms of our vector potential as $\hat{k}_\alpha = -i\partial_\alpha + \frac{el_B}{\hbar c}A_\alpha$. In this treatment, we will use unitless spatial variables (i.e. $\frac{x}{l_B}$ with the magnetic length $l_B = \sqrt{\frac{\hbar c}{eB}}$). In addition, from now on we will express the Hamiltonian and eigenenergies in terms of the cyclotron energy $\hbar\omega = \frac{\hbar eB}{m_0 c}$. We will follow the notation and methods for the analytical portion of the single-particle problem developed in Ref. [45]. The principal concern in the investigation of the 2DHG is taking into consideration of the mutual transformation of heavy and light holes of the hole spectrum upon collisions with the walls of the quantum well [48]. While non-Abelian effects in a single-particle hole spectrum emerge when these mutual transformations are not taken into account [49], and many optical and transport phenomena can be treated when coupling of heavy and light holes in quantum wells are taken into account perturbatively [50–54], an exact analytical approach [45, 48], taking into consideration mutual transformations of holes is important for obtaining spectral crossings that serve as a fertile ground for many-body topological excitations.

In this choice of gauge, the operators $\hat{k}_\alpha$ can be expressed in linear combinations to form ladder operators in the basis of the Landau level wavefunctions for holes with no confinement in a magnetic field, with the familiar commutation relation:

$$\hat{a} = \frac{\hat{k}_x + i\hat{k}_y}{2}, \quad \hat{a}^\dagger = \frac{\hat{k}_x - i\hat{k}_y}{2}; \quad [\hat{a}, \hat{a}^\dagger] = 1. \tag{2.2}$$

These wavefunctions for Landau levels are given as the spatial functions

$$u_{n,k_y}(x) = \frac{1}{\sqrt{2^n n!\sqrt{\pi}}} e^{-\frac{(x-k_y)^2}{2}} H_n(x - k_y), \tag{2.3}$$

where $H_n(x)$ is the n^{th} degree Hermite polynomial. k_y should be thought of as a quantum number for momentum in the $y-$direction, for which the solutions to the Schrödinger equation in the chosen gauge will be plane waves, whereas for the $x-$direction there is localization, as seen in Eq. 2.3. When the $\hat{a}$ and $\hat{a}^\dagger$ operators act on these wavefunctions they have the property of raising and lowering the index n:

$$\hat{a}\ u_{n,k_y}(x) = \sqrt{n-1}\ u_{n-1,k_y}(x); \quad \hat{a}^\dagger\ u_{n,k_y}(x) = \sqrt{n}\ u_{n+1,k_y}(x) \tag{2.4}$$

The Hamiltonian in Eq. 2.1 can then be written in terms of these raising and lowering operators as well as the matrices J_i and the linear combinations $J_\pm = J_x \pm iJ_y$:

$$\begin{aligned}\hat{H} = &\left[\left(\gamma_1 + \frac{5\gamma_2}{2}\right) I - \gamma_2\{J_+, J_-\}\right]\left(\hat{a}^\dagger\hat{a} + \frac{1}{2}\right) + \left[\left(\frac{\gamma_1}{2} + \frac{5\gamma_2}{4}\right) I - \gamma_2 J_z^2\right]\hat{k}_z^2 \\ &- \kappa J_z - q_0 J_z^3 - \sqrt{2}\gamma_3\hat{k}_z\left(\hat{a}^\dagger\{J_+, J_z\} + \hat{a}\{J_-, J_z\}\right) \\ &- \frac{\gamma_2 + \gamma_3}{4}\left[\left(\hat{a}^\dagger\right)^2 J_+^2 + \hat{a}^2 J_-^2\right] - \frac{\gamma_2 - \gamma_3}{4}\left[\left(\hat{a}^\dagger\right)^2 J_-^2 + \hat{a}^2 J_+^2\right] \quad (2.5)\end{aligned}$$

The final two terms in Eq. 2.5 are of slightly different orders of magnitude, due to the values of $\gamma_{2,3}$ that are present in the coefficients. The coefficients for GaAs are $\frac{\gamma_2+\gamma_3}{4} = 1.25$ and $\frac{\gamma_2-\gamma_3}{4} = 0.2$. For these values, it is convenient to neglect the final term, which imposes an axial symmetry about the $z-$direction in which we might choose a convenient basis in which to express the eigenfunctions, which are 4-vector spinors:

$$\mathbf{\Psi}_{n,k_y}(x, y, z) = \begin{pmatrix} \zeta_0(z)u_{n,k_y}(x) \\ \zeta_1(z)u_{n-1,k_y}(x) \\ \zeta_2(z)u_{n-2,k_y}(x) \\ \zeta_3(z)u_{n-3,k_y}(x) \end{pmatrix} e^{ik_y y}. \quad (2.6)$$

The structure of this ansatz wavefunction is compelling because there are multiple Landau level wavefunctions represented for $n > 0$. These quasihole Landau levels have different spin characteristics, and the individual states $\mathbf{\Psi}_{n,k_y}(x, y, z)$ contain mixtures of various percentages of these Landau level states. The $\zeta_i(z)$ functions represent the wavefunction envelope in the z confinement direction. Originally, Luttinger's used the fact that the narrow confinement in the quantum well or heterostructure would make anything but the ground state inaccessible, and the solutions to the Hamiltonian in Ref. [44] to the Schrödinger equation using the Hamiltonian in Eq. 2.1 include the nonphysical $\hat{k}_z \to \infty$, and neglects motion in the $z-$direction. We will determine the shape of the $z-$envelope functions numerically. It should be noted that values of n in the eigenfunction should be restricted to $n \geq 0$. In addition, when a value of n would make the index of one of the $u_{n-j,k_y}(x)$ functions have a negative index, we will take

it to be zero, since in general, these represent solutions to the harmonic oscillator-like hole in a magnetic field.

In this basis, the axially approximated Hamiltonian takes on the following form (again due to Ref. [45]):

$$\hat{H}_z = \begin{pmatrix} \frac{\hat{k}_z^2}{2m_h^z} + P_1 + Z_1 & \Gamma_1\hat{k}_z & A_1 & 0 \\ \Gamma_1\hat{k}_z & \frac{\hat{k}_z^2}{2m_l^z} + P_2 + Z_2 & 0 & A_2 \\ A_1 & 0 & \frac{\hat{k}_z^2}{2m_l^z} + P_2 - Z_2 & \Gamma_2\hat{k}_z \\ 0 & A_2 & \Gamma_2\hat{k}_z & \frac{\hat{k}_z^2}{2m_h^z} + P_1 - Z_1 \end{pmatrix} \tag{2.7}$$

$P_1 = (\gamma_1 + \gamma_2)(n-1),\ P_2 = (\gamma_1 - \gamma_2)(n-1),\ A_1 = -\frac{\gamma_2+\gamma_3}{2}\sqrt{3n(n-1)},\ A_2 = -\frac{\gamma_2+\gamma_3}{2}\sqrt{3(n-1)(n-2)},\ \Gamma_1 = -\gamma_3\sqrt{6n},\ \Gamma_2 = \gamma_3\sqrt{6(n-2)},\ Z_1 = \frac{3(\gamma_1+\gamma_2)}{2} - \frac{3\kappa}{2} - \frac{27q_0}{8}$,

$Z_2 = \frac{\gamma_1-\gamma_2}{2} - \frac{\kappa}{2} - \frac{q_0}{8},\ m_h^z = (\gamma_1 - 2\gamma_2)^{-1},\ m_l^z = (\gamma_1 + 2\gamma_2)^{-1}$ Analytic solutions are possible, but we are in search of solutions with an externally applied electric field. Introduction of this field produces an additional term on the diagonal of the $\hat{H}_z$ matrix. At this point, the Hamiltonian matrix has acted on the $x-$dependent portion of the wavefunction, and while it does not interact with the $y-$dependence (the $y-$direction solutions are free hole solutions, i.e. plane waves), the $z-$dependence can be represented in the 4-vector:

$$\mathbf{Z}(z) = \begin{pmatrix} \zeta_0(z) \\ \zeta_1(z) \\ \zeta_2(z) \\ \zeta_3(z) \end{pmatrix} \tag{2.8}$$

With the vector $\mathbf{Z}(z)$ in this form we may interpret our time-independent Schrödinger equation $\hat{H}_z\mathbf{Z}(z) = E\mathbf{Z}(z)$ as four coupled, second order differential equations for the functions $\zeta_i(z)$. In this vein we may write our Hamiltonian

$$\hat{H}_z = \begin{pmatrix} -\frac{1}{2m_h^z} & 0 & 0 & 0 \\ 0 & -\frac{1}{2m_l^z} & 0 & 0 \\ 0 & 0 & -\frac{1}{2m_l^z} & 0 \\ 0 & 0 & 0 & -\frac{1}{2m_l^z} \end{pmatrix} \frac{\partial^2}{\partial z^2} + \begin{pmatrix} 0 & -i\Gamma_1 & 0 & 0 \\ -i\Gamma_1 & 0 & 0 & 0 \\ 0 & 0 & 0 & -i\Gamma_2 \\ 0 & 0 & -i\Gamma_2 & 0 \end{pmatrix} \frac{\partial}{\partial z}$$
$$+ \begin{pmatrix} P_1 + Z_1 + eEz & 0 & A_1 & 0 \\ 0 & P_2 + Z_2 + eEz & 0 & A_2 \\ A_1 & 0 & P_2 - Z_2 + eEz & 0 \\ 0 & A_2 & 0 & P_1 - Z_1 + eEz \end{pmatrix}. \quad (2.9)$$

with the inclusion of the electric field term in the properly scaled units $\frac{eEx}{\hbar\omega}$. We will absorb the $\hbar\omega$ into the electric field magnitude as above in Eq. 2.9. We will consider electric fields on the order of $E \sim 10^4 - 10^6 \frac{V}{m}$ for our numerical calculations.

In order to evaluate Schrödinger's equation with the Hamiltonian in Eq. 2.9 we need to employ a numerical method of solving differential equations. There are several options, but we will proceed with a finite difference method. In this method, we divide the region or domain within our quantum well of width $2w$ ($z \in [-w, w]$) in which we wish to solve these differential equations into N equally sized subdivisions, of width $a = \frac{2w}{N}$ at where the k^{th} subdivision would be the interval $z \in [z_k, z_{k+1}]$, $z_k = -w + ka$.[1]

[1]The number of subdivisions (N) that we choose will have two side effects: first, it will impose a numerical upper limit on the energy levels that the $z-$dependent portion of the Schrödinger equation will be able to elucidate. If we imagine that the maximum possible spatial frequency will be bounded by the amount $\frac{\pi}{a}$ then we can imagine that there might be a corresponding energy limit. The second side effect of our choice is simply the resolution with which we will see the wavefunction, or more accurately, the modulus squared, $|\zeta_i(z)|^2$.

This choice of method of numerical solution changes the form of the derivatives of $\zeta_i(z)$ to the form

$$\left.\frac{\partial^2\zeta_i(z)}{\partial z^2}\right|_{z=z_k} \approx \frac{1}{a^2}\left[\zeta_i(z_{k+1}) + \zeta_i(z_{k-1}) - 2\zeta_i(z_k)\right]$$
$$\left.\frac{\partial\zeta_i(z)}{\partial z}\right|_{z=z_k} \approx \frac{1}{2a}\left[\zeta_i(z_{k+1}) - \zeta_i(z_{k-1})\right]. \tag{2.10}$$

With this, the Schrödinger equation $\hat{H}_z\mathbf{\Psi}(z)\Big|_{z=z_k} = E_z\mathbf{\Psi}(z)\Big|_{z=z_k}$ takes the form of an algebraic equation, namely

$$\begin{aligned}\hat{H}_z\begin{pmatrix}\zeta_0(z)\\ \zeta_1(z)\\ \zeta_2(z)\\ \zeta_3(z)\end{pmatrix} &= \left[A\frac{\partial^2}{\partial z^2} + B\frac{\partial}{\partial z} + C(z)\right]\begin{pmatrix}\zeta_0(z)\\ \zeta_1(z)\\ \zeta_2(z)\\ \zeta_3(z)\end{pmatrix} \\ \underset{z=z_k}{\longrightarrow} &\left(\frac{1}{a^2}A + \frac{1}{2a}B\right)\begin{pmatrix}\zeta_0(z_{k+1})\\ \zeta_1(z_{k+1})\\ \zeta_2(z_{k+1})\\ \zeta_3(z_{k+1})\end{pmatrix} + \left(\frac{1}{a^2}A - \frac{1}{2a}B\right)\begin{pmatrix}\zeta_0(z_{k-1})\\ \zeta_1(z_{k-1})\\ \zeta_2(z_{k-1})\\ \zeta_3(z_{k-1})\end{pmatrix} \\ &+ \left(-\frac{2}{a^2}A + C(z_k)\right)\begin{pmatrix}\zeta_0(z_k)\\ \zeta_1(z_k)\\ \zeta_2(z_k)\\ \zeta_3(z_k)\end{pmatrix} = E\begin{pmatrix}\zeta_0(z_k)\\ \zeta_1(z_k)\\ \zeta_2(z_k)\\ \zeta_3(z_k)\end{pmatrix}. \end{aligned} \tag{2.11}$$

The matrices A, B, and $C(z)$ are the 4×4 coefficient matrices from Eq. 2.9; while A and B have only constant elements, but $C(z)$ contains the electric field diagonal terms, and is thus dependent on the spatial variable in the confinement direction. Eq. 2.11, when taken at all the subdivisions of the quantum well z_k, $k\in[0,N]$, recasts the four coupled differential equations for $\zeta_i(z)$ in Eq. 2.9 as $4(N+1)$ coupled linear equations for $\zeta_i(z_k)$, $i=0,1,2,3$, $k=0,1,\ldots,N$. These equations are solvable using any linear algebra software, and they produce eigenvalues that are the energies E_z (FIG. 2.1) of the corresponding eigenvectors $\zeta_i(z_k)$ (FIG. 2.2). The $4(N+1)\times 4(N+1)$

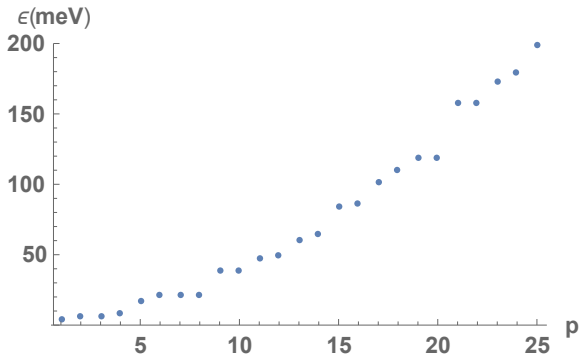

Figure 2.1. Eigenenergies of finite difference method for $n = 3$. "p" quantum number on horizontal axis indexes excited states, with $p = 1$ indicating the ground state of the $n = 3$

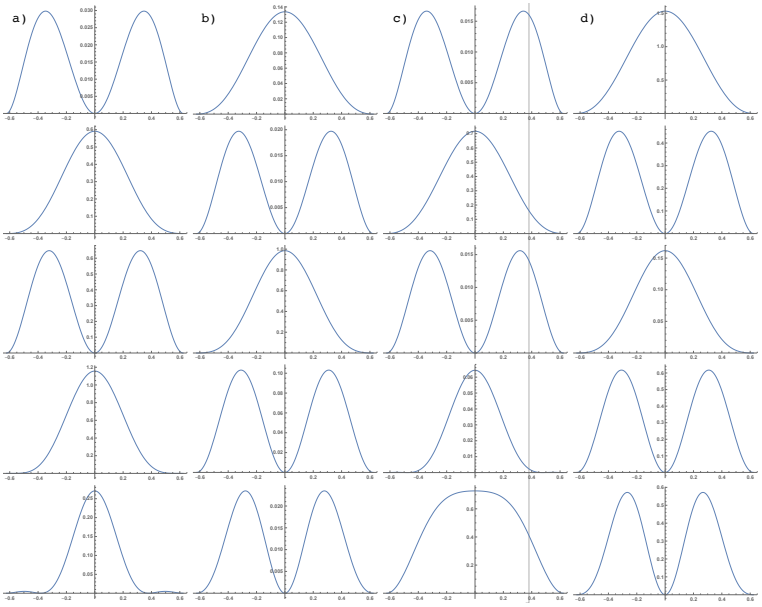

Figure 2.2. $|\zeta_i(z)|^2$ from finite difference method with $N = 100$, $w = 0.623$, $E = 0$. a.) $i = 0$, heavy hole, b.) $i = 1$, light hole, c.) $i = 2$, light hole, d.) $i = 3$, heavy hole. $p = 1, 2, 3, 4, 5$ are shown here.

matrix whose eigenvalues and eigenvectors must be determined is shown in Eq. 2.12 on page 12.

$$\begin{pmatrix}
\frac{-2}{a^2}A + C(z_0) & \frac{1}{a^2}A + \frac{1}{2a}B & 0 & \dots & \dots & \dots & \dots & \dots & 0 \\
\frac{1}{a^2}A - \frac{1}{2a}B & \frac{-2}{a^2}A + C(z_1) & \frac{1}{a^2}A + \frac{1}{2a}B & 0 & & & & & \vdots \\
0 & \frac{1}{a^2}A - \frac{1}{2a}B & \ddots & \ddots & 0 & & & & \vdots \\
\vdots & 0 & \ddots & \frac{-2}{a^2}A + C(z_{k-1}) & \frac{1}{a^2}A + \frac{1}{2a}B & 0 & & & \vdots \\
\vdots & & 0 & \frac{1}{a^2}A - \frac{1}{2a}B & \frac{-2}{a^2}A + C(z_k) & \frac{1}{a^2}A + \frac{1}{2a}B & & & \vdots \\
\vdots & & & 0 & \frac{1}{a^2}A - \frac{1}{2a}B & \frac{-2}{a^2}A + C(z_{k+1}) & \ddots & & \vdots \\
\vdots & & & & & \ddots & \ddots & \frac{1}{a^2}A + \frac{1}{2a}B & 0 \\
\vdots & & & & & 0 & \frac{1}{a^2}A - \frac{1}{2a}B & \frac{-2}{a^2}A + C(z_{N-1}) & \frac{1}{a^2}A + \frac{1}{2a}B \\
0 & \dots & \dots & \dots & \dots & \dots & 0 & \frac{1}{a^2}A - \frac{1}{2a}B & \frac{-2}{a^2}A + C(z_N)
\end{pmatrix} \tag{2.12}$$

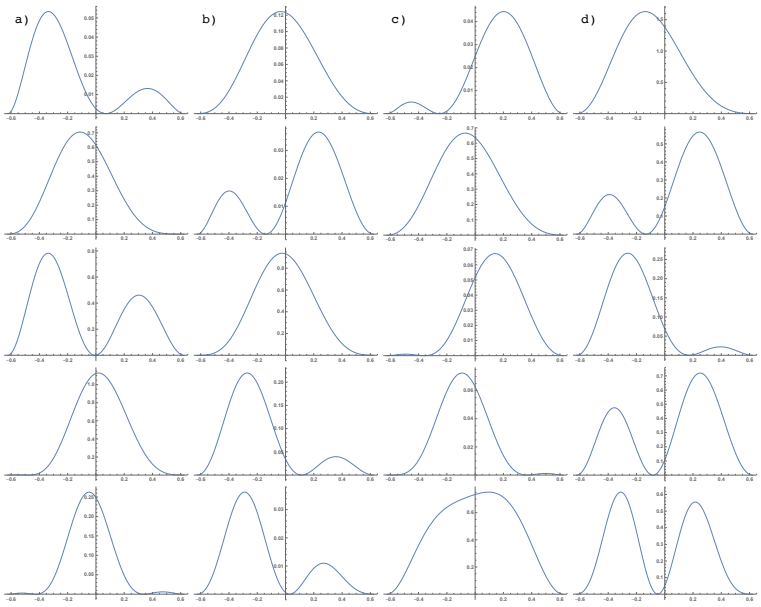

Figure 2.3. $|\zeta_i(z)|^2$ from finite difference method with $N = 100$, $w = 0.623$, $E = 6\frac{kV}{cm}$. a.) $i = 0$, heavy hole, b.) $i = 1$, light hole, c.) $i = 2$, light hole, d.) $i = 3$, heavy hole. $p = 1, 2, 3, 4, 5$ are shown again. Shift in probability density due to externally applied electric field.

The finite difference method can also be applied to a system in an externally applied electric field, as in FIG. 2.3. One may observe the wavefunction is pushed to one side of the quantum well in the lowest lying states, with some higher energy states compensating by shifting in the opposite direction.

The advantage to the ability to tune the system via an externally applied electric field is that it is not difficult from an engineering standpoint. Thus, with a sufficiently wide quantum well it is possible to directly tune the tunneling coupling between two quasi-layers just by applying an external gate voltage.

2.2 Energy Levels at Various Magnetic Field Values

Because the spatial coordinate has been expressed as a unitless quantity scaled by the magnetic length $l_B = \sqrt{\frac{\hbar c}{eB}}$, and the width of the quantum well has been expressed

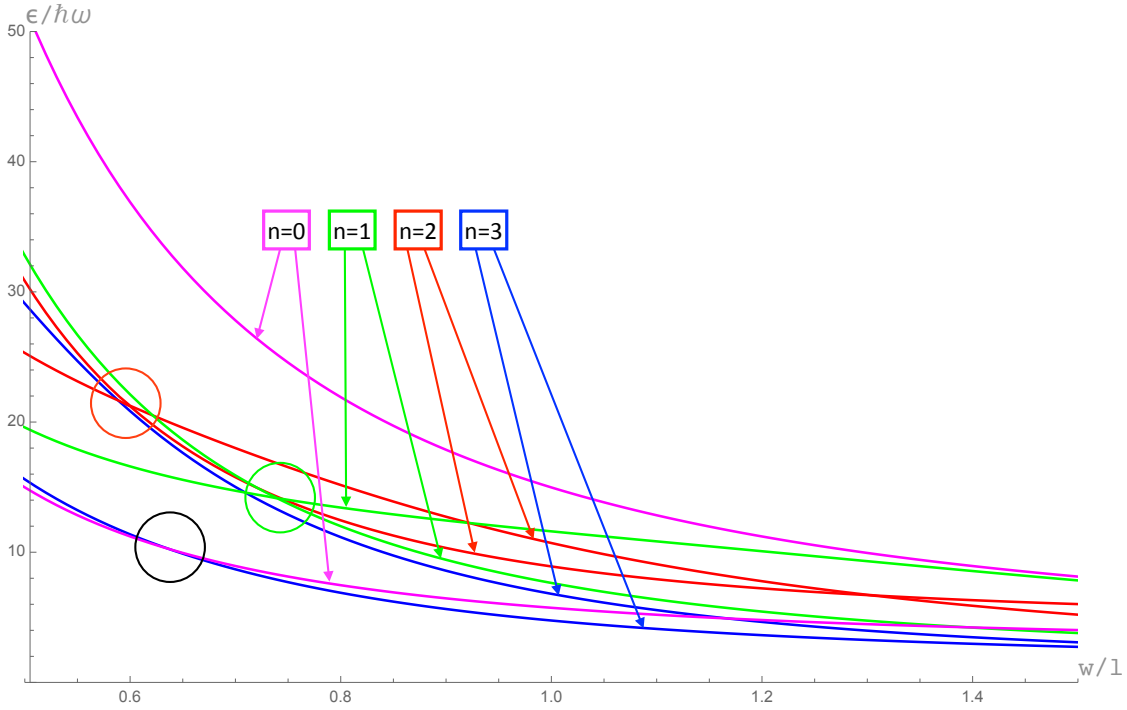

Figure 2.4. Energy levels for two lowest lying eigenenergies for $n = 0, 1, 2, 3$ at various values of well width. Blue lines are $n = 3$, red lines are $n = 2$, green lines are $n = 1$, and magenta lines are $n = 0$.Various crossings between different n energy levels (e.g. black circle between $n = 3$ and $n = 0$ ground states near $\frac{w}{l_B} = 0.64$), as well as within a given n (e.g. green and red circles for crossings between $n = 1$ and $n = 2$ states near $\frac{w}{l_B} = 0.60$ and $\frac{w}{l_B} = 0.75$, respectively).

in these coordinates, the effect of changing the width of the quantum well is to in some sense change the magnetic field strength ($\frac{w}{l_B} \propto \sqrt{B}$). This can be understood by considering the classical picture of a quantum well of fixed width. In this scenario, increasing the magnetic field would create more localized classical cyclotron orbits with smaller radii.

To this end we might consider investigating various n values, which index the $x-$direction Landau level wavefunctions. Investigating the $n = 0, 1, 2, 3$ lowest lying energy levels, we can attempt to determine which state is the ground state for various values of the magnetic field strength, i.e. well width (FIG. 2.4). Crossings in the

spectrum show different n states as the ground state for different values of B, or well width $\frac{w}{l_B}$. These features are one of the compelling advantages of investigating the hole spectrum in semiconductors, as the spectrum of electrons in equivalent systems would not exhibit such crossings, in the absence of a strong Zeeman splitting due to an in-plane magnetic field (for $\nu = \frac{2}{3}$ for example, since $\nu = \frac{1}{3}$ is a spin-polarized state in electron systems [30, 33]), or within diluted magnetic semiconductors such as CdMnTe [55]. For our purposes, the crossing between the $n = 0$ and $n = 3$ states at $w/l_B \approx 0.68$ in Fig. 2.4 is particularly interesting. These two states have opposite pseudospin properties, and thus manipulation of a portion of a sample into one or the other ground state gives rise to a strong intrinsic spin-orbit effect. Because of the inherent difficulty in putting spatial variance in magnetic fields of the magnitudes we would require, we will investigate other modes of spatial control of the ground state of our system.

2.3 Manipulation of Ground State Energy Crossings

The search for a manipulable ground state in our system motivates additional examination of the system in a perpendicular electric field. The $z-$envelope single particle densities from Fig. 2.3 display an obvious shift to one side, caused by the introduction of an external gate voltage. Because of the difficulty of imposing a spatially-varying magnetic field on a sample of the size we are considering, it might prove challenging to use a magnetic field variation in order to put different parts of the sample in various regions with respect to the ground state crossing (see Fig. 2.4). This difficulty leads us to instead investigate the energy-dependence of the single particle solutions to the Schrödinger equation upon the gate voltage, given that it is comparably simple to impose different electrostatic top gate voltages at various locations on a physical sample. The effects of an asymmetric or triangular potential well upon the properties of holes in GaAs/AlGaAs valence bands has been studied previously in [56–58], specifically in regard to heterostructure settings.

To this effect, we choose a convenient range of magnetic field values and investigate a few top gate voltage values to determine whether it is in fact possible to manipulate the crossing of the ground states. This is illustrated in Fig. 2.5 in which we can see that the ground state crossing can be moved from higher to lower values of external magnetic field with application of an external gate voltage in the kV/cm range (for a $200\mathring{A}$ wide quantum well).

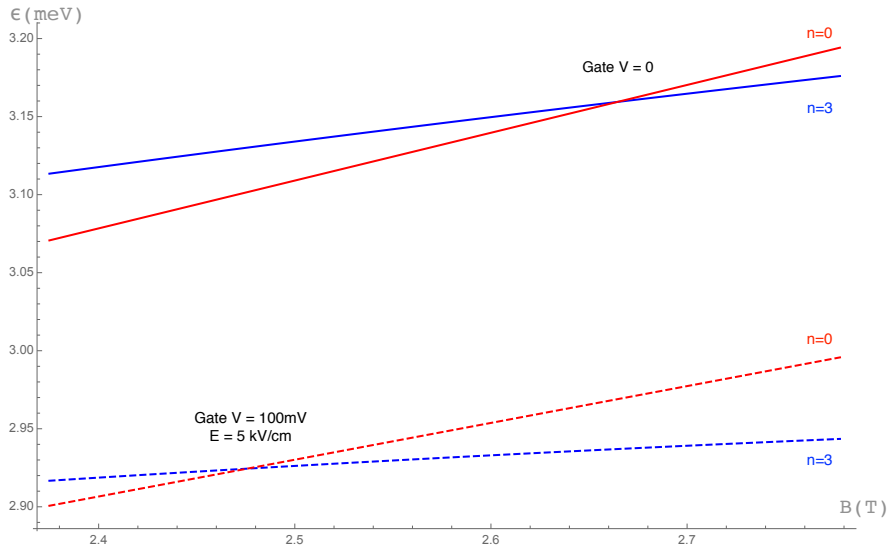

Figure 2.5. Energy of two ground states ($n = 0$, $n = 3$) in external gate voltage-induced electric field $E_g = 0$ and $E_g = 5\ \frac{kV}{cm}$, plotted as a function of magnetic field.

Choosing a vertical slice in the energy vs. magnetic field plot in Fig. 2.5 between the crossing at low and high external gate voltage allows us to monitor the two states' energies as a function of external gate voltage, as in Fig. 2.6. We discover here that at low or zero externally applied E_g the ground state by an interval of about 2 meV is the $n = 0$ state, whereas at larger $|E_g| = 5\ \frac{kV}{cm}$,the $n = 3$ state is lower in energy by a similar margin.

The angular momentum 3/2 nature of our holes (heavy and light holes occupying the $\pm\frac{3}{2}$ and $\pm\frac{1}{2}$ branches, respectively) leads us to question the nature of our

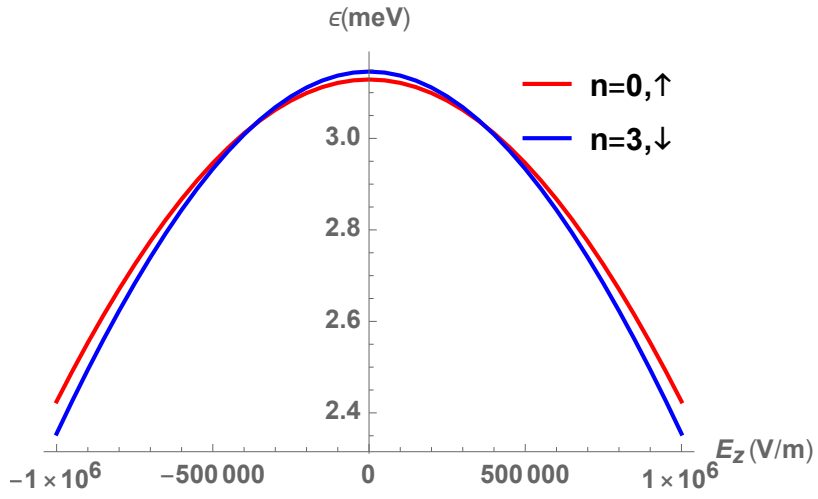

Figure 2.6. Gate-applied E_g dependence of ground state energies.

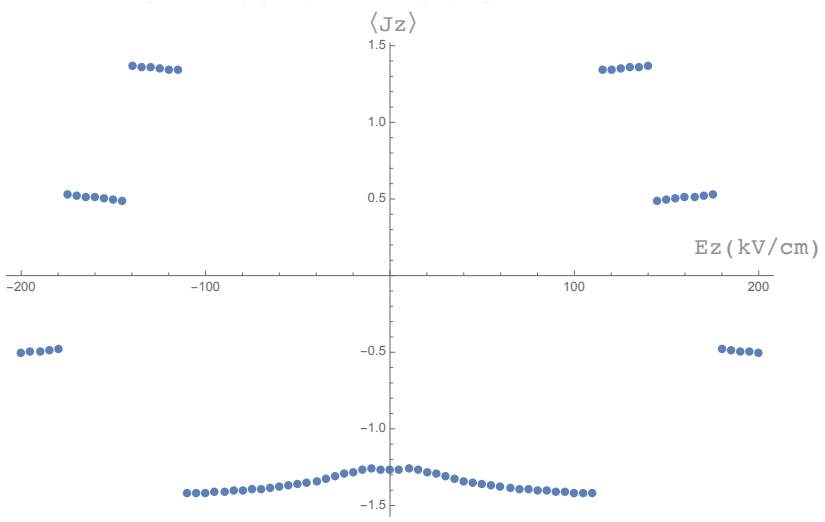

Figure 2.7. $\langle J_z \rangle_{n=3}$ plotted as a function of gate-applied electric field E_g. State maintains its $\langle J_z \rangle \approx -\frac{3}{2}$ character until around $E_g \approx 100\ \frac{kV}{cm}$, well beyond the field values we consider here.

ground states for the purpose of later introducing superconductivity and spin- (angular momentum-) based phenomena. To that effect we can find the expected value of the J_z operator in order to determine the angular momentum projection of our

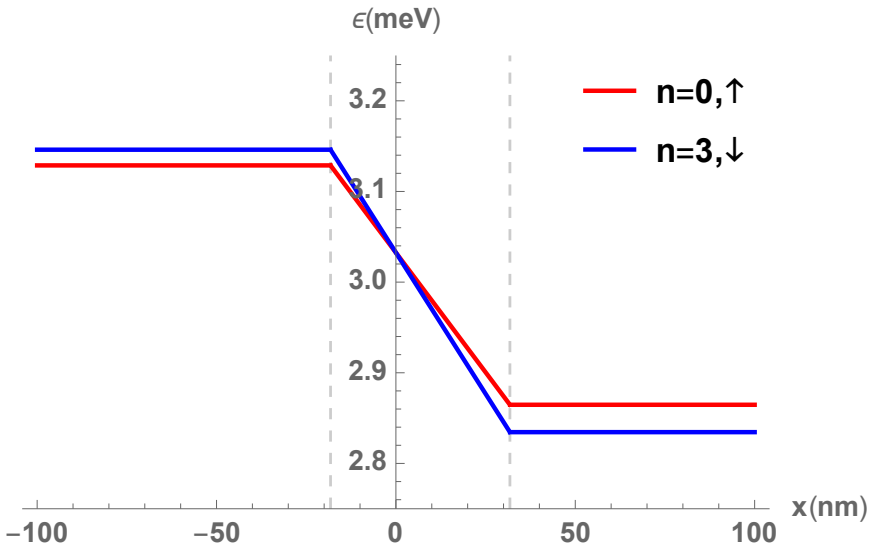

Figure 2.8. A sketch of the $x-$dependence of the ground state energy levels in a 200 nm-wide region between external gate field $E_g = 0$ and $E_g = 6\ \frac{kV}{cm}$, where we have, for the sake of approximation, let the transition between regions occur in a 50 nm-wide region in the center.

$n = 0, 3$ states, given that we predicted that they would exhibit spin up/down characteristics. When doing so we obtain exactly $\langle J_z \rangle = +3/2$ for the $n = 0$ state, as it is a pure state with only one element in its state vector; however, the $n = 3$ state varies somewhat in our electric field, so it will be important to assure ourselves that it remains spin down, generally. The $\langle J_z \rangle_{n=3}$ value is shown in Fig. 2.7.

In some sense this confirms the use of the $n = 0, 3$ ground states as pseudospin $\pm\frac{3}{2}$ states, which will be useful as we proceed, as we will attempt to realize a system in which one part of our sample is under no gate voltage, and another is under some externally applied electric field, so that somewhere in between these two regions our ground states cross, as we sketch in Fig. 2.8. In our sketched sample, the different slopes of our ground state energies as a function of the spatial coordinates will lead to edge currents in the crossing region of different velocities for the $n = 0, 3$ species, although they will co-propagate.

3. INTERACTIONS ON A CYLINDER

3.1 Coulomb Interaction in a Cylindrical Geometry

We must investigate the effect of particle-particle interactions in order to fully understand the nature of the ground state of our system. Historically, the fractional quantum hall effect in electron systems has been realized by exact diagonalization of the Coulomb interaction between few particles in several geometries: originally done by Haldane on the sphere after the original wavefunction formulation by Laughlin [59, 60], later expanded upon by Fano, Ortolani, and Colombo [61]; shortly thereafter by Halperin on the disk [62]. The disk geometry makes possible to investigate the effect of the finite width of the quantum well and include the effects of Landau level mixing [63, 64]. Later, Haldane and Rezayi formulated the problem within a system with periodic boundary conditions in two directions, i.e. a toroidal geometry [65], and eventually one with only one periodic direction with a confining potential in the other, i.e. a cylindrical system [66].

Quantum Hall effects in a system of two-dimensional charge carrier holes have been considered in [67]. A spherical shell geometry was used there in numerical simulation of interaction effects and quantum Hall states. Spherical shell geometry allows to take into account strong coupling between the spin and motion of charge parallel and perpendicular to the 2D layer that characterizes charge carrier holes in two dimensions.

In this work we choose to work in a cylindrical shell, adding a dimension of thickness in the direction perpendicular to the plane of the 2DHS. The method of applying Haldane pseudopotentials to observe FQHE edge states has been used before in a cylindrical geometry with hard core interactions in [68]. Similar to the spherical shell geometry [67] the cylinder allows one to capture the coupling of spin to transverse

and in-plane hole motion, with a more natural extension to the study of edges. Account of coupling of heavy and light hole branches in the single-particle spectrum also allows us to capture these effects on the many-body level via computing Haldane pseudopotentials.

The Coulomb interaction in second quantization is of the form:

$$\sum_{\substack{n_1,m_1,p_1;\\ n_2,m_2,p_2;\\ n_3,m_3,p_3;\\ n_4,m_4,p_4}} V^{n_3,m_3,p_3;n_4,m_4,p_4}_{n_1,m_1,p_1;n_2,m_2,p_2} c^\dagger_{n_1,m_1,p_1} c^\dagger_{n_2,m_2,p_2} c_{n_3,m_3,p_3} c_{n_4,m_4,p_4} \ , \tag{3.1}$$

where $c^{(\dagger)}_{n_i,m_i,p_i}$ are annihilation (creation) operators for holes with x quantum number n_i indexing the Landau Level wavefunction, y quantum number m_i indexing angular momentum, and p_i indexing the z direction confinement envelope. We start with wavefunctions from the previous section, again expressed in coordinates that are in units of the magnetic length $l_b = \sqrt{\frac{\hbar c}{eB}}$

$$\mathbf{\Psi}(x,y,z)_{n,k_y} = \begin{pmatrix} \zeta_0(z) u_{n,k_y}(x) \\ \zeta_1(z) u_{n-1,k_y}(x) \\ \zeta_2(z) u_{n-2,k_y}(x) \\ \zeta_3(z) u_{n-3,k_y}(x) \end{pmatrix} e^{ik_y y} \ , \tag{2.6}$$

where $u_{n,k_y}(x)$ is a Landau Level wavefunction:

$$u_{n,k_y}(x) = \frac{1}{\sqrt{2^n n! \sqrt{\pi}}} e^{-\frac{(x-k_y)^2}{2}} H_n(x-k_y) \ , \tag{2.4}$$

with $H_n(x)$ a Hermite polynomial of degree n (refer to Section 2.1). We put our system into a cylindrical geometry where the y-direction is the circumferential, the x-direction is the length, and the z-direction is the thickness of the cylindrical shell. The periodic boundary condition on the circumferential direction (with circumference L) requires that

$$e^{ik_y L} = 1 \tag{3.2}$$

And so we have

$$k_y L = 2\pi m, \ m \in \mathbb{Z} \ . \tag{3.3}$$

We can express the matrix element $V^{n_3,m_3,p_3;n_4,m_4,p_4}_{n_1,m_1,p_1;n_2,m_2,p_2}$ in terms of these wavefunctions in energy units of $\frac{e^2}{\epsilon_R l_b}$:

$$
\begin{aligned}
V^{n_3,m_3,p_3;n_4,m_4,p_4}_{n_1,m_1,p_1;n_2,m_2,p_2} &= \langle \Psi_{n_1,m_1,p_1}(\mathbf{r}_1)\Psi_{n_2,m_2,p_2}(\mathbf{r}_2)| \, \frac{1}{|\mathbf{r}_1-\mathbf{r}_2|} \, |\Psi_{n_3,m_3,p_3}(\mathbf{r}_2)\Psi_{n_4,m_4,p_4}(\mathbf{r}_1)\rangle \\
&= \int d\mathbf{r}_1 d\mathbf{r}_2 \frac{\left(\Psi^\dagger_{n_1,m_1,p_1}(\mathbf{r}_1)\Psi^\dagger_{n_2,m_2,p_2}(\mathbf{r}_2)\Psi_{n_3,m_3,p_3}(\mathbf{r}_2)\Psi_{n_4,m_4,p_4}(\mathbf{r}_1)\right)}{|\mathbf{r}_1-\mathbf{r}_2|} \\
&= \frac{1}{\left(\sqrt{L\sqrt{\pi}}\right)^4} \int d\mathbf{r}_1 d\mathbf{r}_2 \frac{e^{-\frac{1}{2}\left[(x_1-\frac{2\pi m_1}{L})^2+(x_2-\frac{2\pi m_2}{L})^2+(x_2-\frac{2\pi m_3}{L})^2+(x_1-\frac{2\pi m_4}{L})^2\right]}}{|\mathbf{r}_1-\mathbf{r}_2|} \\
&\sum_{j,k=0}^{3} \frac{e^{-i\frac{2\pi}{L}(m_1-m_4)y_1 - i\frac{2\pi}{L}(m_2-m_3)y_2}\left(\zeta^*_{n_1,p_1,j}(z_1)\zeta_{n_4,p_4,j}(z_1)\zeta^*_{n2,p_2,k}(z_2)\zeta_{n_3,p_3,k}(z_2)\right)}{\sqrt{2^{n_1+n_2+n_3+n_4-2k-2j}(n_1-j)!(n_2-k)!(n_3-k)!(n_4-j)!}} \\
&\qquad H_{n_1-j}\left(x_1-\frac{2\pi m_1}{L}\right) H_{n_4-j}\left(x_1-\frac{2\pi m_4}{L}\right) \\
&\qquad\qquad H_{n_2-k}\left(x_2-\frac{2\pi m_2}{L}\right) H_{n_3-k}\left(x_2-\frac{2\pi m_3}{L}\right) \quad . \quad (3.4)
\end{aligned}
$$

Again, n_i labels the Landau level, m_i the y-direction circumferential (periodic) confinement, and p_i indexes the envelope of the wavefunction in the z-direction.

In our example we must examine N_s states, with N holes, in filling factor ν ($\nu = \frac{1}{3}$ for our purposes). The number of states is then $N_s = \nu^{-1}N - S$, where $S = 2$ because we are examining polarized states (unpolarized states like the $\nu = \frac{2}{3}$ have $S = 0$) specifically on the cylinder [69]. This bound on the number of states constrains our values of m_i such that $0 \leq m_i < N_s$. Once we have put N particles in N_s states, we must constrain the length of the cylinder we consider in order to maintain the particle density. This constraint forces the length of the cylinder to be $\frac{2\pi N_s}{L}$, such that the total surface area of the cylinder is $2\pi N_s$, and the particle density is $\frac{N}{2\pi N_s}$. This is reminiscent of the relationship between areal particle density and filling vactor: $n = \frac{\nu}{2\pi l_B}$, where l_B is the magnetic length (in our units, $l_B = 1$, so $n = \frac{\nu}{2\pi}$). Our value varies from this one because of the S which is due to polarization.

Treating the $1/|\mathbf{r}_1 - \mathbf{r}_2|$ term is simpler if we take the two-dimensional (nonunitary) Fourier transform:

$$\mathcal{F}\left\{\frac{1}{|\mathbf{r}_1 - \mathbf{r}_2|}\right\}(k_x, k_y) = \mathcal{F}\left\{\frac{1}{\sqrt{(x_1-x_2)^2 + (y_1-y_2)^2 + (z_1-z_2)^2}}\right\}(k_x, k_y)$$
$$\to \int_{-\infty}^{\infty}\int_{-\infty}^{\infty} \frac{e^{-i(k_x x + k_y y)}}{\sqrt{x^2+y^2+z^2}} dx dy \to \int_0^{\infty} r dr \int_0^{2\pi} d\theta \left[\frac{e^{-ir(k_x\cos\theta + k_y \sin\theta)}}{\sqrt{r^2+z^2}}\right] , \quad (3.5)$$

where we have transformed to cylindrical coordinates in the usual way. Making an additional substitution:

$$\cos\phi = \frac{k_x}{k}, \ \sin\phi = \frac{k_y}{k}$$
$$k_x \cos\theta + k_y \sin\theta = k(\cos\theta\cos\phi + \sin\theta\sin\phi) = k\cos(\theta - \phi) ,$$

we get the transformation

$$\int_0^{\infty} r dr \int_0^{2\pi} d\theta \left[\frac{e^{-irk\cos(\theta-\phi)}}{\sqrt{r^2+z^2}}\right] = 2\pi \int_0^{\infty} \frac{r J_0(kr)}{\sqrt{r^2+z^2}} dr . \quad (3.6)$$

where $J_0(x)$ is the 0th order Bessel function of the first kind, obtained by evaluation of the angular integral. This last integral is that of a modified Bessel function of the second kind $K_\alpha(x)$:

$$\int_0^{\infty} \frac{t^{\nu+1} J_\nu(at)}{(t^2+b^2)^{\mu+1}} dt = \frac{a^\mu b^{\nu-\mu}}{2^\mu \Gamma(\mu+1)} K_{\nu-\mu}(ab) \ \text{ [NIST HMF 10.22.46] [70] .} \quad (3.7)$$

Using the substitutions $\nu = 0$, $\mu = -\frac{1}{2}$, $a = k$, $b = z$ we obtain the following result:

$$2\pi \int_0^{\infty} \frac{r J_0(kr)}{\sqrt{r^2+z^2}} dr = 2\pi \frac{k^{-\frac{1}{2}} z^{\frac{1}{2}}}{2^{-\frac{1}{2}}\Gamma(\frac{1}{2})} K_{\frac{1}{2}}(kz) = 2\pi\sqrt{\frac{2z}{\pi k}}\left(\sqrt{\frac{\pi}{2kz}} e^{-k|z|}\right) = 2\pi \frac{e^{-k|z|}}{k} . \quad (3.8)$$

This allows us to express the Coulomb interaction in terms of the inverse Fourier transform:

$$\frac{1}{\sqrt{x^2+y^2+z^2}} = \frac{1}{(2\pi)^2} \int_{-\infty}^{\infty}\int_{-\infty}^{\infty} 2\pi \frac{e^{-\sqrt{k_x^2+k_y^2}|z| + i(k_x x + k_y y)}}{\sqrt{k_x^2+k_y^2}} dk_x dk_y . \quad (3.9)$$

Putting this into the above expression:

$$V_{n_1,m_1,p_1;n_2,m_2,p_2}^{n_3,m_3,p_3;n_4,m_4,p_4} = \frac{1}{2L^2\pi^2}\int d\mathbf{r}_1 d\mathbf{r}_2 dk_x dk_y \frac{e^{-\sqrt{k_x^2+k_y^2}|z_1-z_2|+i(k_x(x_2-x_1)+k_y(y_2-y_1))}}{\sqrt{k_x^2+k_y^2}}$$
$$e^{-\frac{1}{2}\left[(x_1-\frac{2\pi m_1}{L})^2+(x_2-\frac{2\pi m_2}{L})^2+(x_2-\frac{2\pi m_3}{L})^2+(x_1-\frac{2\pi m_4}{L})^2\right]}$$
$$\sum_{j,k=0}^{3} \frac{e^{-i\frac{2\pi}{L}(m_1-m_4)y_1-i\frac{2\pi}{L}(m_2-m_3)y_2}\left(\zeta^*_{n_1,p_1,j}(z_1)\zeta_{n_4,p_4,j}(z_1)\zeta^*_{n_2,p_2,k}(z_2)\zeta_{n_3,p_3,k}(z_2)\right)}{\sqrt{2^{n_1+n_2+n_3+n_4-2k-2j}(n_1-j)!(n_2-k)!(n_3-k)!(n_4-j)!}}$$
$$H_{n_1-j}\left(x_1-\frac{2\pi m_1}{L}\right)H_{n_4-j}\left(x_1-\frac{2\pi m_4}{L}\right)$$
$$H_{n_2-k}\left(x_2-\frac{2\pi m_2}{L}\right)H_{n_3-k}\left(x_2-\frac{2\pi m_3}{L}\right) \ . \quad (3.10)$$

We might isolate the y_1-, y_2-, and k_y-dependent portions of the expression:

$$\int_{-\infty}^{\infty} dk_y \int_{-\infty}^{\infty} dy_1 \int_{-\infty}^{\infty} dy_2 \frac{e^{-\sqrt{k_x^2+k_y^2}|z_1-z_2|+ik_y(y_2-y_1)-i\frac{2\pi}{L}(m_1-m_4)y_1-i\frac{2\pi}{L}(m_2-m_3)y_2}}{\sqrt{k_x^2+k_y^2}} \ . \quad (3.11)$$

The bounds of the y_1 and y_2 integrations are set to $\pm\infty$ although the cylinder's circumference is L because the interactions between holes continues after more than one time around the cylinder, with holes interaction with their own and other holes' images ad infinitum. This interaction of the tail of the wavefunction with an infinite number of images is technically divergent, a singularity that we will later subtract from our interaction integral.

So we may rearrange the expression to find Dirac delta functions from the y_1 and y_2 integrals:

$$= \int_{-\infty}^{\infty} dk_y \left\{ \frac{e^{-\sqrt{k_x^2+k_y^2}|z_1-z_2|}}{\sqrt{k_x^2+k_y^2}} \left(\int_{-\infty}^{\infty} e^{i\left(\frac{2\pi}{L}(m_4-m_1)-k_y\right)y_1} dy_1 \right) \right. \quad (3.12)$$
$$\left. \left(\int_{-\infty}^{\infty} e^{i\left(\frac{2\pi}{L}(m_3-m_2)+k_y\right)y_2} dy_2 \right) \right\}$$
$$= (2\pi)^2 \int_{-\infty}^{\infty} \frac{e^{-\sqrt{k_x^2+k_y^2}|z_1-z_2|}}{\sqrt{k_x^2+k_y^2}} \left[\delta\left(\frac{2\pi}{L}(m_4-m_1)-k_y\right) \delta\left(\frac{2\pi}{L}(m_3-m_2)+k_y\right) \right] dk_y$$
$$= 2\pi L \frac{e^{-\sqrt{k_x^2+\left(\frac{2\pi}{L}\right)^2(m_4-m_1)^2}|z_1-z_2|}}{\sqrt{k_x^2+\left(\frac{2\pi}{L}\right)^2(m_4-m_1)^2}} \delta_{m_4-m_1,m_3-m_2} \ .$$

(3.13)

The Kronecker delta arises as a consequence of the product of two Dirac delta functions in the second line of the above equation. If the m_i do not satisfy this relationship, the Dirac delta functions would be centered at different values of k_y in the integrand, and the value of the integral would be zero. We interpret this Kronecker delta $\delta_{m_4-m_1,m_3-m_2}$ as an enforcement of conservation of momentum in our interaction.

We must now address the x_1 and x_2 integrals. Examining first the x_1 expression:

$$\int_{-\infty}^{\infty}\left[e^{-ik_x x_1-\frac{1}{2}\left(x_1-\frac{2\pi m_1}{L}\right)^2-\frac{1}{2}\left(x_1-\frac{2\pi m_4}{L}\right)^2}H_{n_1-j}\left(x_1-\frac{2\pi m_1}{L}\right)H_{n_4-j}\left(x_1-\frac{2\pi m_4}{L}\right)\right]dx_1\ . \tag{3.14a}$$

Making some substitutions for succinctness, we let $a=\frac{2\pi m_1}{L}$, $b=\frac{2\pi m_4}{L}$, $m=n_1-j$, $n=n_4-j$:

$$\int_{-\infty}^{\infty}\left[e^{-ik_x x-\frac{1}{2}(x-a)^2-\frac{1}{2}(x-b)^2}H_m(x-a)H_n(x-b)\right]dx\ . \tag{3.14b}$$

Some manipulations of the exponential into a single Gaussian with a complex argument gives us:

$$e^{-\frac{1}{4}k_x^2-\frac{1}{2}ik_x(a+b)-\frac{1}{4}(a-b)^2}\int_{-\infty}^{\infty}\left[e^{-\left(x-\frac{1}{2}(a+b-ik_x)\right)^2}H_m(x-a)H_n(x-b)\right]dx\ . \tag{3.15a}$$

A new substitution becomes necessary: $u=x-\frac{1}{2}(a+b-ik_x)$:

$$e^{-\frac{1}{4}k_x^2-\frac{1}{2}ik_x(a+b)-\frac{1}{4}(a-b)^2}\int_{-\infty+ik_x}^{\infty+ik_x}\left[e^{-u^2}H_m\left(u+\frac{1}{2}(b-a-ik_x)\right)H_n\left(u+\frac{1}{2}(a-b-ik_x)\right)\right]du\ . \tag{3.15b}$$

It may appear that the complex bounds complicate the problem somewhat, but examining the integrand, we find a Gaussian function and Hermite polynomials, both of which are analytic everywhere in the complex plane. Thus there are no poles we must consider. If we then consider the region in the upper half-plane bounded by the rectangular contour defined by $\{u\in\mathbb{C}:\Re(u)\in[-R,R],\ \Im(u)\in[0,k_x]\}$, in the limit where $R\to\infty$, the Gaussian component of the integrand suppresses the value of any

polynomial at large R. Thus the vertical portions of the contour integral approach zero as $R \to \infty$, and given the analyticity of the integrand, we may set the offset portion of the contour integral equal to the portion on the real axis.

Evaluation of this integral is due to Gradshteyn and Ryzhik (1943) Eqn. [7.377] [71]:

$$\int_{-\infty}^{\infty} e^{-x^2} H_m(x+y) H_n(x+z) dx = 2^n \sqrt{\pi} m! z^{n-m} L_m^{(n-m)}(-2yz) \quad (n \geq m) \ , \quad (3.16)$$

where $L_n^{(a)}(x)$ is the associated Laguerre polynomial. Applying this formula while allowing for either m or n in our expression to be greater, we obtain the following result for the real axis-shifted version of (3.15b):

$$\begin{aligned} e^{-\frac{1}{4}k_x^2 - \frac{1}{2}ik_x(a+b) - \frac{1}{4}(a-b)^2} \int_{-\infty}^{\infty} \Bigg[& e^{-u^2} H_m\left(u + \frac{1}{2}(b-a-ik_x)\right) \\ & H_n\left(u + \frac{1}{2}(a-b-ik_x)\right)\Bigg] du \\ = e^{-\frac{1}{4}k_x^2 - \frac{1}{2}ik_x(a+b) - \frac{1}{4}(a-b)^2} & 2^{min(m,n)} \sqrt{\pi} [min(m,n)]! \\ (sgn(n-m)(b-a) - ik_x)^{|n-m|} & L_{min(m,n)}^{(|n-m|)}\left(-\frac{1}{2}(b-a-ik_x)(a-b-ik_x)\right) \ . \end{aligned} \quad (3.17)$$

Substituting back in we obtain an expression in terms of the original parameters:

$$\begin{aligned} & e^{-\left(\frac{\pi}{L}\right)^2 (m_1-m_4)^2 - ik_x\left(\frac{\pi}{L}\right)(m_1+m_4) - \frac{1}{4}k_x^2} 2^{min(n_1,n_4)-j} \sqrt{\pi} [min(n_1,n_4)-j]! \\ & \left(sgn(n_1-n_4)\frac{2\pi}{L}(m_1-m_4) - ik_x\right)^{|n_1-n_4|} L_{min(n_1,n_4)-j}^{(|n_1-n_4|)}\left(\frac{k_x^2}{2} + \frac{2\pi^2}{L^2}(m_1-m_4)^2\right) \ . \end{aligned} \quad (3.18)$$

In order to evaluate the x_2 integral we need just make the following transformations: $k_x \to -k_x$, $(m_1, n_1) \to (m_2, n_2)$, $(m_4, n_4) \to (m_3, n_3)$, $j \to k$.

After some rearrangement of the factorial terms and exponents we may now re-express our interaction matrix:

$$V^{n_3,m_3,p_3;n_4,m_4,p_4}_{n_1,m_1,p_1;n_2,m_2,p_2} = \frac{\delta_{m_4-m_1,m_3-m_2}}{L}\frac{e^{-\left(\frac{\pi}{L}\right)^2\left[(m_1-m_4)^2+(m_2-m_3)^2\right]}}{\sqrt{2^{|n_1-n_4|+|n_2-n_3|}}}$$
$$\sum_{j,k=0}^{3}\sqrt{\frac{[min(n_1,n_4)-j]![min(n_2,n_3)-k]!}{[max(n_1,n_4)-j]![max(n_2,n_3)-k]!}}\int_{-w}^{w}dz_1\int_{-w}^{w}dz_2\Bigg\{\zeta^*_{n_1,p_1,j}(z_1)\zeta_{n_4,p_4,j}(z_1)$$
$$\zeta^*_{n_2,p_2,k}(z_2)\zeta_{n_3,p_3,k}(z_2)\int_{-\infty}^{\infty}\Bigg[\frac{e^{-\sqrt{k_x^2+\left(\frac{2\pi}{L}\right)^2(m_4-m_1)^2}|z_1-z_2|-\frac{1}{2}k_x^2-ik_x\left(\frac{\pi}{L}\right)(m_1+m_4-m_2-m_3)}}{\sqrt{k_x^2+\left(\frac{2\pi}{L}\right)^2(m_4-m_1)^2}}$$
$$\left(sgn(n_1-n_4)\frac{2\pi}{L}(m_1-m_4)-ik_x\right)^{|n_1-n_4|}$$
$$\left(sgn(n_2-n_3)\frac{2\pi}{L}(m_2-m_3)+ik_x\right)^{|n_2-n_3|}$$
$$L^{(|n_1-n_4|)}_{min(n_1,n_4)-j}\left(\frac{k_x^2}{2}+\frac{2\pi^2}{L^2}(m_1-m_4)^2\right)L^{(|n_2-n_3|)}_{min(n_2,n_3)-k}\left(\frac{k_x^2}{2}+\frac{2\pi^2}{L^2}(m_2-m_3)^2\right)\Bigg]dk_x\Bigg\}\ . \tag{3.19}$$

The bounds of the z-integral, $\pm w$ are the thickness of the 2DEG ($2w$) in units of magnetic length.

3.2 Interaction Pseudopotentials

When we consider the Kronecker delta, we may enforce the conservation of momentum on our interaction matrix. We may then express these matrix elements in terms of specific combinations of our m_i values, $m = m_4 - m_1$ and $m' = m_1 - m_2$:

$$V^{n_3,p_3;n_4,p_4}_{n_1,p_1;n_2,p_2}(m,m') = \frac{e^{-2\left(\frac{\pi m}{L}\right)^2}}{L\sqrt{2^{|n_1-n_4|+|n_2-n_3|}}} \sum_{j,k=0}^{3} \sqrt{\frac{[min(n_1,n_4)-j]![min(n_2,n_3)-k]!}{[max(n_1,n_4)-j]![max(n_2,n_3)-k]!}}$$
$$\int_{-w}^{w} dz_1 \int_{-w}^{w} dz_2 \Bigg\{ \zeta^*_{n_1,p_1,j}(z_1)\zeta_{n_4,p_4,j}(z_1)\zeta^*_{n_2,p_2,k}(z_2)\zeta_{n_3,p_3,k}(z_2) \int_{-\infty}^{\infty} \Bigg[\frac{e^{-\sqrt{k_x^2+\left(\frac{2\pi m}{L}\right)^2}|z_1-z_2|}}{\sqrt{k_x^2+\left(\frac{2\pi m}{L}\right)^2}}$$
$$e^{-\frac{1}{2}k_x^2 - ik_x\left(\frac{2\pi}{L}\right)(m+m')} \left(-sgn(n_1-n_4)\frac{2\pi m}{L} - ik_x\right)^{|n_1-n_4|} \left(sgn(n_2-n_3)\frac{2\pi m}{L} + ik_x\right)^{|n_2-n_3|}$$
$$L^{(|n_1-n_4|)}_{min(n_1,n_4)-j}\left(\frac{k_x^2}{2}+\frac{2\pi^2m^2}{L^2}\right) L^{(|n_2-n_3|)}_{min(n_2,n_3)-k}\left(\frac{k_x^2}{2}+\frac{2\pi^2m^2}{L^2}\right)\Bigg] dk_x \Bigg\} . \quad (3.20)$$

Examining the k_x integral (in square brackets) we must consider the character of the integrand when $m = 0$ and as $k_x \to 0$, where it seems the denominator $\sqrt{k_x^2+\left(\frac{2\pi m}{L}\right)^2} \to 0$ as the numerator remains finite. When $m = 0$, the terms on the third line of the above expression go as $k_x^{|n_1-n_4|+|n_2-n_3|}$, and thus our entire integrand is only singular if $|n_1 - n_4| = |n_2 - n_3| = 0$. At this same point, our z-integrals which contain our envelope functions $\zeta^{(*)}_{n_i,p_i,j}(z)$ also contain the exponential $e^{-\sqrt{k_x^2+\left(\frac{2\pi m}{L}\right)^2}|z_1-z_2|}$, which couples the z_1 and z_2 integrals. At $m = 0$ and $k_x \to 0$, this exponential goes to 1, and the z integrals decouple. At this point, the envelope functions, which are orthogonal,

only integrate to nonzero values when $p_1 = p_4$ and $p_2 = p_3$. At this point in order to remove the singularity we must address the singular part $\frac{\delta_{m+m',0}\delta_{n_1,n_4}\delta_{n_2,n_3}\delta_{p_1,p_4}\delta_{p_2,p_3}}{|k_x|}$:

$$V^{n_3,p_3;n_4,p_4}_{n_1,p_1;n_2,p_2}(m,m') = \frac{e^{-2\left(\frac{\pi m}{L}\right)^2}}{L\sqrt{2^{|n_1-n_4|+|n_2-n_3|}}} \sum_{j,k=0}^{3} \sqrt{\frac{[min(n_1,n_4)-j]![min(n_2,n_3)-k]!}{[max(n_1,n_4)-j]![max(n_2,n_3)-k]!}}$$
$$\int_{-\infty}^{\infty} dk_x \Bigg\{ \frac{e^{-\frac{1}{2}k_x^2}\left(e^{-ik_x\left(\frac{2\pi}{L}\right)(m+m')} - \delta_{m,0}\delta_{n_1,n_4}\delta_{n_2,n_3}\delta_{p_1,p_4}\delta_{p_2,p_3}\right)}{\sqrt{k_x^2 + \left(\frac{2\pi m}{L}\right)^2}}$$
$$\left(-sgn(n_1-n_4)\frac{2\pi m}{L} - ik_x\right)^{|n_1-n_4|} \left(sgn(n_2-n_3)\frac{2\pi m}{L} + ik_x\right)^{|n_2-n_3|}$$
$$L^{(|n_1-n_4|)}_{min(n_1,n_4)-j}\left(\frac{k_x^2}{2} + \frac{2\pi^2 m^2}{L^2}\right) L^{(|n_2-n_3|)}_{min(n_2,n_3)-k}\left(\frac{k_x^2}{2} + \frac{2\pi^2 m^2}{L^2}\right) dk_x$$
$$\int_{-w}^{w} dz_1 \int_{-w}^{w} dz_2 \left[e^{-\sqrt{k_x^2+\left(\frac{2\pi m}{L}\right)^2}|z_1-z_2|} \zeta^*_{n_1,p_1,j}(z_1)\zeta_{n_4,p_4,j}(z_1)\zeta^*_{n_2,p_2,k}(z_2)\zeta_{n_3,p_3,k}(z_2)\right] \Bigg\} . \tag{3.21}$$

Changing variables in our k_x integral to $x = \frac{k_x}{\sqrt{2}}$ we have the following:

$$V^{n_3,p_3;n_4,p_4}_{n_1,p_1;n_2,p_2}(m,m') =$$
$$\frac{e^{-2\left(\frac{\pi m}{L}\right)^2}}{\sqrt{2}L\sqrt{2^{|n_1-n_4|+|n_2-n_3|}}} \sum_{j,k=0}^{3} \sqrt{\frac{[min(n_1,n_4)-j]![min(n_2,n_3)-k]!}{[max(n_1,n_4)-j]![max(n_2,n_3)-k]!}}$$
$$\int_{-\infty}^{\infty} dx \Bigg\{ \frac{e^{-x^2}\left(e^{-ix\left(\frac{\sqrt{2}\pi}{L}\right)(m+m')} - \delta_{m,0}\delta_{n_1,n_4}\delta_{n_2,n_3}\delta_{p_1,p_4}\delta_{p_2,p_3}\right)}{\sqrt{2x^2 + \left(\frac{2\pi m}{L}\right)^2}}$$
$$\left(-sgn(n_1-n_4)\frac{2\pi m}{L} - i\sqrt{2}x\right)^{|n_1-n_4|} \left(sgn(n_2-n_3)\frac{2\pi m}{L} + i\sqrt{2}x\right)^{|n_2-n_3|}$$
$$L^{(|n_1-n_4|)}_{min(n_1,n_4)-j}\left(x^2 + \frac{2\pi^2 m^2}{L^2}\right) L^{(|n_2-n_3|)}_{min(n_2,n_3)-k}\left(x^2 + \frac{2\pi^2 m^2}{L^2}\right) dk_x$$
$$\int_{-w}^{w} dz_1 \int_{-w}^{w} dz_2 \left[e^{-\sqrt{2x^2+\left(\frac{2\pi m}{L}\right)^2}|z_1-z_2|} \zeta^*_{n_1,p_1,j}(z_1)\zeta_{n_4,p_4,j}(z_1)\zeta^*_{n_2,p_2,k}(z_2)\zeta_{n_3,p_3,k}(z_2)\right] \Bigg\} . \tag{3.22}$$

Because the wavefunction envelopes in the z-direction are calculated numerically on a grid of spacing $a = \frac{2w}{N}$ where N is adjusted to provide resolution as needed, the z-integrals may also be calculated from those numerical results:

$$I^{n_3,p_3;n_4,p_4}_{n_1,p_1;n_2,p_2}(x,m) = \int_{-w}^{w} dz_1 \int_{-w}^{w} dz_2 \Bigg[e^{-\sqrt{2x^2+\left(\frac{2\pi m}{L}\right)^2}|z_1-z_2|} \times \zeta^*_{n_1,p_1,j}(z_1)\zeta_{n_4,p_4,j}(z_1)\zeta^*_{n_2,p_2,k}(z_2)\zeta_{n_3,p_3,k}(z_2) \Bigg]$$
$$\approx a^2 \sum_{\alpha,\beta=0}^{N} e^{-\sqrt{2x^2+\left(\frac{2\pi m}{L}\right)^2}|z_\alpha - z_\beta|} \zeta^*_{n_1,p_1,j}(z_\alpha)\zeta_{n_4,p_4,j}(z_\alpha)\zeta^*_{n_2,p_2,k}(z_\beta)\zeta_{n_3,p_3,k}(z_\beta) \ . \quad (3.23)$$

This $I^{n_3,p_3;n_4,p_4}_{n_1,p_1;n_2,p_2}(x,m)$ can be calculated for various values of x and m, but we still must evaluate the x integral, which is of the form, generally speaking:

$$\int_{-\infty}^{\infty} e^{-x^2} f(x) dx \ . \quad (3.24)$$

When $f(x)$ is relatively well behaved, integrals of this form may be numerically evaluated using Gauss-Hermite quadrature:

$$\int_{-\infty}^{\infty} e^{-x^2} f(x) dx = \sum_{q=1}^{n} w_q f(x_q) + R_n$$
$$w_q = \frac{2^{n-1} n! \sqrt{\pi}}{n^2 [H_{n-1}(x_q)]^2} \quad R_n = \frac{n!\sqrt{\pi}}{2^n (2n)!} f^{(2n)}(\xi) \quad (-\infty < \xi < \infty) \ . \quad (3.25)$$

The w_q are our weights, the remainder is R_n which is typically small, and the abscissas x_q are the q'th zero of the Hermite polynomial $H_n(x)$, which can be either determined analytically for small n or solved for numerically. In general, choosing a larger value

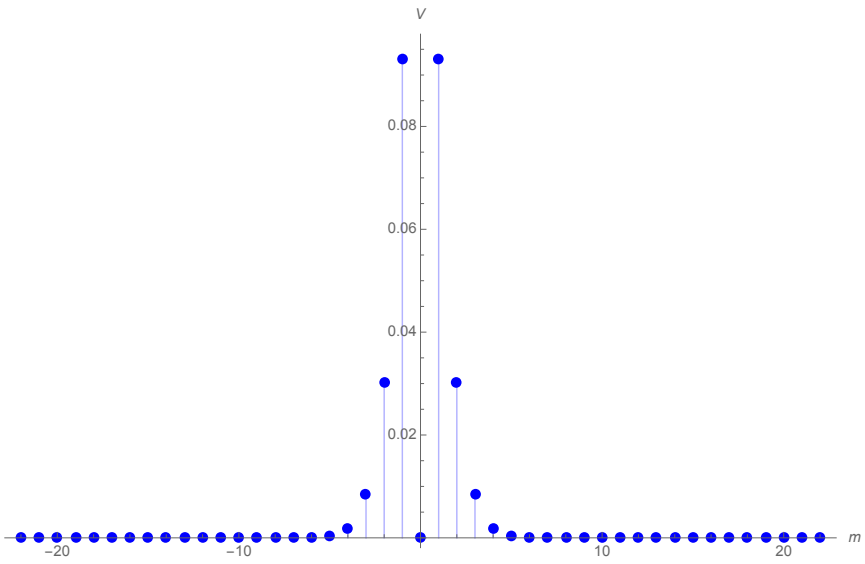

Figure 3.1. Haldane pseudopotentials $V(m, m' = 0)$ for $n_1 = n_2 = n_3 = n_4 = 0$, for $N = 8$ interacting holes ($m = -22, \ldots, 22$). Note that $V(0, 0) = 0$, and the value of V quickly drops for $|m| > 1$.

of n in the above finite sum will allow the sum to converge to the integral's value, thus we may rewrite our interaction matrix

$$V^{n_3,p_3;n_4,p_4}_{n_1,p_1;n_2,p_2}(m,m') = \frac{e^{-2\left(\frac{\pi m}{L}\right)^2}}{\sqrt{2}L\sqrt{2^{|n_1-n_4|+|n_2-n_3|}}} \sum_{j,k=0}^{3} \sqrt{\frac{[min(n_1,n_4)-j]![min(n_2,n_3)-k]!}{[max(n_1,n_4)-j]![max(n_2,n_3)-k]!}} \sum_{q=0}^{n} \left\{ \frac{w_q \left(e^{-ix_q\left(\frac{\sqrt{2}\pi}{L}\right)(m+m')} - \delta_{m,0}\delta_{n_1,n_4}\delta_{n_2,n_3}\delta_{p_1,p_4}\delta_{p_2,p_3} \right)}{\sqrt{2x_q^2 + \left(\frac{2\pi m}{L}\right)^2}} \left(-sgn(n_1-n_4)\frac{2\pi m}{L} - i\sqrt{2}x_q \right)^{|n_1-n_4|} \left(sgn(n_2-n_3)\frac{2\pi m}{L} + i\sqrt{2}x_q \right)^{|n_2-n_3|} L^{(|n_1-n_4|)}_{min(n_1,n_4)-j}\left(x_q^2 + \frac{2\pi^2 m^2}{L^2} \right) L^{(|n_2-n_3|)}_{min(n_2,n_3)-k}\left(x_q^2 + \frac{2\pi^2 m^2}{L^2} \right) I^{n_3,p_3;n_4,p_4}_{n_1,p_1;n_2,p_2}(x_q,m) \right\} . \quad (3.26)$$

where w_q and x_q are defined above in Eq. (3.25).

With this expression we have a reasonable ability to calculate interaction between a number of holes on the order of $N = 10$ as a function of m and m'. These matrix elements are referred to in the literature as pseudopotentials, or Haldane pseudopotentials (shown in FIG. 3.1). The value of V tends to drop off sharply for $|m| > 1$, and is nonexistent for $m = m' = 0$.[1] Our strategy now is to find an appropriate basis in which to diagonalize our interaction effects, so as to see the energy spectrum near the ground state of our two-dimensional hole liquid system.

[1]For computational simplicity, it should be noted that one may use a synthetic pseudopotential by setting $V(m, m') = \delta_{|m|,1}$ with the proper scaling to see some of the structure of the interaction spectrum.

4. THE CONFIGURATION-INTERACTION APPROACH

4.1 Center of Mass/Momentum Basis for Interaction Calculation

Our approach to a basis in which to diagonalize the Coulomb interaction pseudopotential effects in our two-dimensional hole liquid is what we will refer to as a center of momentum (COM) basis (following Ref. [72]). It has been alternative or more generally termed a configuration-interaction calculation, a method of common use in physics and chemistry for calculating interactions in microscopic systems [61]. The $N-$particle basis consists of the various combinations of momentum quantum numbers m_i for which the sum of is some given number M, i.e.

$$\sum_{i=1}^{N} m_i = M \ . \tag{4.1}$$

This basis can be expressed either in an occupation basis $|n_0, n_1, \ldots, n_{N_s}\rangle$ where n_i is the number of holes in the state with momentum quantum number $m = i$ (where $0 \leq m \leq N_s$). It could alternatively be expressed in the form $|m_1, m_2, \ldots, m_N\rangle$, where the m_i are just the momentum quantum numbers of each of the holes. Because of the Pauli exclusion principle, the m_i must be distinct.

The problem we are approaching is similar to the computer science question of the k-subset sum problem, in which one finds the subsets of a certain set of elements with length k that all have a common sum M. Our k is the number of particles N, and our set from which we build our subsets is the possible m values that our holes might have for N particles[1] such that their sum is M. Given the repulsive nature of the Coulomb interaction, it is reasonable to assume the ground state to be the most evenly spaced subset. With this assumption we can form the hypothesis that the ground state energy occurs for the state, in occupation basis $|1, 0, 0, 1, 0, 0, \ldots, 0, 1, 0, 0, 1\rangle$ or in the $\{m_i\}$

[1]Recall from the previous section on interactions that the m values vary between $0, 1, \ldots, N_s$ where $N_s = \nu^{-1}N - 2$ for the cylindrical geometry.

basis, $|0, 3, 6, \ldots, N_s - 1 = 3(N-1)\rangle$, for the cylinder with N holes. Our motivation from this comes from the form of the $x-$dependent portion of the wavefunction, which are Hermite functions (Eq. 2.3), the eigenfunctions of a harmonic oscillator potential, but centered at the various locations $k_y = \frac{2\pi m}{L}$. This state exhibits the largest possible separation between respective holes. This state has a total momentum quantum number

$$M_L = \sum_{i=1}^{N} m_i = 0 + 3 + 6 + \ldots + 3(N-1) = \sum_{i=1}^{N} 3(i-1)$$
$$= 3\left(\sum_{i=1}^{N} i - \sum_{i=1}^{N} 1\right) = 3\left(\frac{N(N+1)}{2} - N\right) = \frac{3}{2}N(N-1)\ . \quad (4.2)$$

This gives, for example, $N = 6$ particles, a total momentum quantum number $M_L = 45$, and $N = 10$ particles, $M_L = 135$, etc. Our hypothesis is that this will be the ground state of our system after applying interaction effects, and that this should then have high overlap with the Laughlin state for N particles.

If we look for other states with $M = M_L$, we will find that there are many, many such states, that number increasing wildly for increasing N. For instance, with $N = 6$ particles, there are 338 states with $M = M_L = 45$, but with $N = 10$ particles, $M_L = 135$, the number of states with the same M is $246,448$. The number of states with the "Laughlin" sum M_L seems to be a symmetric maximum, decreasing with a variation in M in either direction from M_L. The computational problem of generating all the necessary subsets to form a basis for a given N, M is significant, but will be set aside in this work.

Once the subset is generated, the next step is to calculate interaction matrix elements in a basis of these subsets. Again, one may see why the number of subsets increasing quickly is a computation challenge, with the interaction matrix going from 338×338 to $246,448 \times 246,448$ for $N = 6$ to $N = 10$ particles, effectively increasing the number of matrix elements from 10^5 to $10^{10} - 10^{11}$. That said, with suitably sparse matrices, there are methods for procuring a diagonalization for at least a significant subset of the eigenvalues of these matrices.

At this point we must examine the structure of this interaction matrix. The elements will be of the form

$$\langle m'_1, m'_2, \ldots, m'_N | \, \hat{V}_C(\mathbf{r}_1, \mathbf{r}_2, \ldots, \mathbf{r}_N) \, | m_1, m_2, \ldots, m_N \rangle \, , \text{ where } \hat{V}_C = \sum_{i<j}^{N} \frac{1}{|\mathbf{r}_i - \mathbf{r}_j|}. \tag{4.3}$$

The state $|m_1, m_2, \ldots, m_N\rangle = |\{m_i\}_N\rangle$ is a Slater determinants of the single particle wavefunctions with momentum quantum numbers $\{m_i\}$,

$$|m_1, m_2, \ldots, m_N\rangle = \frac{1}{\sqrt{N!}} \begin{vmatrix} \mathbf{\Psi}_{m_1}(\mathbf{r}_1) & \mathbf{\Psi}_{m_2}(\mathbf{r}_1) & \ldots & \mathbf{\Psi}_{m_N}(\mathbf{r}_1) \\ \mathbf{\Psi}_{m_1}(\mathbf{r}_2) & \mathbf{\Psi}_{m_2}(\mathbf{r}_2) & \ldots & \mathbf{\Psi}_{m_N}(\mathbf{r}_2) \\ \vdots & \vdots & \ddots & \vdots \\ \mathbf{\Psi}_{m_1}(\mathbf{r}_N) & \mathbf{\Psi}_{m_2}(\mathbf{r}_N) & \ldots & \mathbf{\Psi}_{m_N}(\mathbf{r}_N) \end{vmatrix} . \tag{4.4}$$

This equation can be written in a more compact form by making use of the permutation group $S(N)$ and its elements σ. For $N = 3$, a given subset, e.g. $|0, 3, 6\rangle$ would have permutations $\sigma = [1, 2, 3]$, the identity, and positive permutations $\sigma = [3, 1, 2], [2, 3, 1]$ along with negative permutations $\sigma = [1, 3, 2], [2, 1, 3], [3, 2, 1]$, for a total of 6 permutations (the same as the number $N!$). The sign of the permutation $sgn(\sigma)$ is obtained by determining the number of times one must swap holes in order to get from the identity to the desired σ permutation. The Slater determinant for a general N hole state can then be written

$$|m_1, m_2, \ldots, m_N\rangle = \frac{1}{\sqrt{N!}} \sum_{\sigma \in S(N)} \left(sgn(\sigma) \prod_{i=1}^{N} \mathbf{\Psi}_{m_i}(\mathbf{r}_{\sigma_i}) \, . \right). \tag{4.5}$$

The above example $|0,3,6\rangle$ then has the Slater determinant form

$$
\begin{aligned}
|0,3,6\rangle &= \frac{1}{\sqrt{3!}} \sum_{\sigma \in S(3)} \left(sgn(\sigma) \prod_{i=1}^{3} \mathbf{\Psi}_{m_i}(\mathbf{r}_{\sigma_i}) \right) \\
&= \frac{1}{\sqrt{3!}} \Big[sgn([1,2,3]) \mathbf{\Psi}_0(\mathbf{r}_1) \mathbf{\Psi}_3(\mathbf{r}_2) \mathbf{\Psi}_6(\mathbf{r}_3) \\
&+ sgn([2,3,1]) \mathbf{\Psi}_0(\mathbf{r}_2) \mathbf{\Psi}_3(\mathbf{r}_3) \mathbf{\Psi}_6(\mathbf{r}_1) + sgn([3,1,2]) \mathbf{\Psi}_0(\mathbf{r}_3) \mathbf{\Psi}_3(\mathbf{r}_1) \mathbf{\Psi}_6(\mathbf{r}_2) \\
&+ sgn([1,3,2]) \mathbf{\Psi}_0(\mathbf{r}_1) \mathbf{\Psi}_3(\mathbf{r}_3) \mathbf{\Psi}_6(\mathbf{r}_2) + sgn([2,1,3]) \mathbf{\Psi}_0(\mathbf{r}_2) \mathbf{\Psi}_3(\mathbf{r}_1) \mathbf{\Psi}_6(\mathbf{r}_3) \\
&+ sgn([3,2,1]) \mathbf{\Psi}_0(\mathbf{r}_3) \mathbf{\Psi}_3(\mathbf{r}_2) \mathbf{\Psi}_6(\mathbf{r}_1) \Big] \\
&= \frac{1}{\sqrt{6}} \Big[\mathbf{\Psi}_0(\mathbf{r}_1) \mathbf{\Psi}_3(\mathbf{r}_2) \mathbf{\Psi}_6(\mathbf{r}_3) + \mathbf{\Psi}_0(\mathbf{r}_2) \mathbf{\Psi}_3(\mathbf{r}_3) \mathbf{\Psi}_6(\mathbf{r}_1) + \mathbf{\Psi}_0(\mathbf{r}_3) \mathbf{\Psi}_3(\mathbf{r}_1) \mathbf{\Psi}_6(\mathbf{r}_2) \\
&- \mathbf{\Psi}_0(\mathbf{r}_1) \mathbf{\Psi}_3(\mathbf{r}_3) \mathbf{\Psi}_6(\mathbf{r}_2) - \mathbf{\Psi}_0(\mathbf{r}_2) \mathbf{\Psi}_3(\mathbf{r}_1) \mathbf{\Psi}_6(\mathbf{r}_3) - \mathbf{\Psi}_0(\mathbf{r}_3) \mathbf{\Psi}_3(\mathbf{r}_2) \mathbf{\Psi}_6(\mathbf{r}_1) \Big] \ . \quad (4.6)
\end{aligned}
$$

With this notation, a general element in the interaction matrix from Eq. 4.3 has the form

$$
\begin{aligned}
&\langle m'_1, m'_2, \ldots, m'_N | \, \hat{V}_C(\mathbf{r}_1, \mathbf{r}_2, \ldots, \mathbf{r}_N) \, | m_1, m_2, \ldots, m_N \rangle = \\
&\quad = \langle \{m'_i\}_N | \, \hat{V}_C \, | \{m_j\}_N \rangle = \frac{1}{N!} \sum_{\sigma' \in S(N)} \sum_{\sigma \in S(N)} sgn(\sigma') sgn(\sigma) \\
&\qquad \times \int \left(\prod_{i=1}^{N} \mathbf{\Psi}^{\dagger}_{m'_i}(\mathbf{r}_{\sigma'_i}) \right) \sum_{\alpha < \beta}^{N} \frac{1}{|\mathbf{r}_\alpha - \mathbf{r}_\beta|} \left(\prod_{j=1}^{N} \mathbf{\Psi}_{m_j}(\mathbf{r}_{\sigma_j}) \right) d^N \mathbf{r} \ . \quad (4.7)
\end{aligned}
$$

If we pick the two states $\mathbf{\Psi}^{(\dagger)}_{m_i^{(\prime)}}(\mathbf{r}_{\sigma_i^{(\prime)}})$ from each of the products within the integrand in Eq. 4.7 for which the coordinate matches those coordinates in the interaction and separate that integral from those that go over the non-interacting coordinates (for that particular term), we can write two distinct parts of the interaction matrix element. We will choose to signify the coordinates from the term in the sum that we have arbitrarily picked as $\mathbf{r}_\delta$ and $\mathbf{r}_\gamma$, and display that single term from the sum in the interaction:

$$
\begin{aligned}
&\frac{sgn(\sigma') sgn(\sigma)}{N!} \int \left(\prod_{i \neq k,l}^{N} \mathbf{\Psi}^{\dagger}_{m'_i}(\mathbf{r}_{\sigma'_i}) \right) \left(\prod_{j \neq q,r}^{N} \mathbf{\Psi}_{m_j}(\mathbf{r}_{\sigma_j}) \right) d^{(N-2)} \mathbf{r} \\
&\qquad \times \int \mathbf{\Psi}^{\dagger}_{m'_k}(\mathbf{r}_\gamma) \mathbf{\Psi}^{\dagger}_{m'_l}(\mathbf{r}_\delta) \frac{1}{|\mathbf{r}_\gamma - \mathbf{r}_\delta|} \mathbf{\Psi}_{m_q}(\mathbf{r}_\delta) \mathbf{\Psi}_{m_r}(\mathbf{r}_\gamma) d\mathbf{r}_\delta d\mathbf{r}_\gamma \ . \quad (4.8)
\end{aligned}
$$

Given this term, it should be noted that a second, almost identical term exists, except the coordinates are switched for the non$-\dagger$ wavefunctions.[2] The $sgn(\sigma)$ for this term with swapped coordinates differs from the expression in Eq. 4.8 by exactly one permutation, and so it picks up a minus sign relative to the term in Eq. 4.8, i.e.

$$\frac{sgn(\sigma')sgn(\sigma)}{N!}\int\left(\prod_{i\neq k,l}^{N}\mathbf{\Psi}^{\dagger}_{m'_i}(\mathbf{r}_{\sigma'_i})\right)\left(\prod_{j\neq q,r}^{N}\mathbf{\Psi}_{m_j}(\mathbf{r}_{\sigma_j})\right)d^{(N-2)}\mathbf{r}$$
$$\times\left[\int\mathbf{\Psi}^{\dagger}_{m'_k}(\mathbf{r}_\gamma)\mathbf{\Psi}^{\dagger}_{m'_l}(\mathbf{r}_\delta)\frac{1}{|\mathbf{r}_\gamma-\mathbf{r}_\delta|}\mathbf{\Psi}_{m_q}(\mathbf{r}_\delta)\mathbf{\Psi}_{m_r}(\mathbf{r}_\gamma)d\mathbf{r}_\delta d\mathbf{r}_\gamma\right.$$
$$\left.-\int\mathbf{\Psi}^{\dagger}_{m'_k}(\mathbf{r}_\gamma)\mathbf{\Psi}^{\dagger}_{m'_l}(\mathbf{r}_\delta)\frac{1}{|\mathbf{r}_\gamma-\mathbf{r}_\delta|}\mathbf{\Psi}_{m_q}(\mathbf{r}_\gamma)\mathbf{\Psi}_{m_r}(\mathbf{r}_\delta)d\mathbf{r}_\delta d\mathbf{r}_\gamma\right]. \quad (4.9)$$

The elements of σ and σ', which we've labeled σ_j and σ'_i, are different permutations of the same set of consecutive integers from the permutation group $S(N)$, and thus we may assume that within the products in the first integral of Eq. 4.9, the same coordinates will be present. For all terms for which the corresponding coordinates in the first integrand in this equation are paired with non-identical m'_i, m_j values, the first integral, and thus the whole term, will vanish due to the orthogonality of the wavefunctions. For the remaining terms in which for any $\sigma'_i = \sigma_j$, the corresponding m values obey $m'_i = m_j$, the orthonormality of the wavefunctions will cause the first integral to evaluate to unity, leaving only the $sgn(\sigma)$ term and the interaction integrals to evaluate. If the only non-zero terms of the sort represented in Eq. 4.9 are those for which these conditions are satisfied, then we can start to see that a matrix made up of sums of these elements will have many zero entries. In fact, we have suggested here that the only terms that do not vanish are the ones for which at least $N-2$ of the N values of m for each of the states are identical. Additionally, given the requirement of the conserved COM (Eq. 4.1) the remaining two terms inside the interaction integrals have somewhat strict requirements that they are either equal (either $m'_k = m_q$, and m'_l=m_r, or alternatively $m'_k = m_r$ and $m'_l = m_q$) or that they

[2]Either the $\dagger$ or non$-\dagger$ terms could swap coordinates, but it is redundant to swap both, and additionally, the $\alpha < \beta$ requirement from the original sum in Eq. 4.7 prevents the double-swapped term from existing.

are completely distinct, but still add up to the same number (since all other values of m are equal and the remainder of the sum M is the same for both terms). In the former case in which the m quantum numbers are respectively equal, the term in question must be a diagonal element in which $\{m'_i\} = \{m_j\}$. In the latter case in which the interacting terms are distinct, this is an off-diagonal matrix element. The off-diagonal term reduces when non-zero to the expression

$$\frac{sgn(\sigma')sgn(\sigma)}{N!}\left[V(m'_k - m_r, m'_k - m_q) - V(m'_k - m_q, m'_k - m_r)\right] \ , \tag{4.10}$$

where the $V(m, m')$ are the interaction matrix elements from Section 3. When the term is a diagonal term, additional non-zero elements must be considered, since there will be multiple terms in the interaction potential for which a term of the form in Eq. 4.9 can be written. This diagonal term will then take the form

$$\frac{1}{N!}\sum_{\alpha<\beta}\left[V(m_\alpha - m_\alpha, m_\alpha - m_\beta) - V(m_\alpha - m_\beta, m_\alpha - m_\alpha)\right]$$
$$= \frac{1}{N!}\sum_{\alpha<\beta}\left[V(0, m_\alpha - m_\beta) - V(m_\alpha - m_\beta, 0)\right] \ . \tag{4.11}$$

The $sgn(\sigma)$ term can disappear because $[sgn(\sigma)]^2 = 1$ for any permutation, and the only non-zero terms in the diagonal elements will be the ones with the identical permutation σ, and those with exactly one swapped element (the first and second terms in Eq. 4.11, respectively).

The structure of the diagonal and off-diagonal elements of the interaction matrix in the conserved COM basis can be executed computationally, and eigenvalues can be found via direct or numerical methods, depending on the size of the matrix.[3]

[3]Recall that the number of subsets of size N with sum M grow very quickly with increasing N and M, and thus the number of elements that must be calculated, though much smaller than the number of subsets squared, also increases with N and M.

4.2 Parabolic Confinement and the Gap

It is prudent at this juncture to note that the sample we have constructed to interact on the cylinder is limited in the circumferential direction to a length L, but is not physically limited in the length direction, at least mathematically.[4] To formally confine the holes, we can introduce a synthetic confinement potential of a shape that we choose, in this case, a $1D$ parabolic confinement

$$\hat{V}_{conf}(\mathbf{r}_1, \ldots, \mathbf{r}_N) = a \sum_{i=1}^{N} x_i^2 \ . \tag{4.12}$$

We must either inject this potential into the original Hamiltonian on the diagonal elements and then reevaluate the single-particle solution, or we may investigate the matrix elements of this interaction in the COM basis from Section 4. The former destroys the structure of our interaction picture, so let us investigate the matrix elements of $\hat{V}_{conf}$ in the basis of conserved COM.

Our matrix elements have the form

$$\begin{aligned} \langle \{m_i'\} | \, \hat{V}_{conf} \, | \{m_j\} \rangle = & \sum_{\sigma' \in S(N)} \sum_{\sigma \in S(N)} \frac{sgn(\sigma')sgn(\sigma)}{N!} \\ & \times \int \left(\prod_{i=1}^{N} \mathbf{\Psi}^{\dagger}_{m_i'}(\mathbf{r}_{\sigma_i'}) \right) \left(a \sum_{k=1}^{N} x_k^2 \right) \left(\prod_{j=1}^{N} \mathbf{\Psi}_{m_j}(\mathbf{r}_{\sigma_j}) \right) d^N\mathbf{r} \ , \end{aligned} \tag{4.13}$$

following the notation from Section 4. Again, we may investigate terms in the sum over k in the integrand in Eq. 4.13 individually in order to ascertain whether some may be zero due to orthogonality requirements. One such term is

$$a \frac{sgn(\sigma')sgn(\sigma)}{N!} \int \left(\prod_{i \neq k}^{N} \mathbf{\Psi}^{\dagger}_{m_i'}(\mathbf{r}_{\sigma_i'}) \prod_{j \neq l}^{N} \mathbf{\Psi}_{m_j}(\mathbf{r}_{\sigma_j}) \right) d^{(N-1)}\mathbf{r} \int \left(\mathbf{\Psi}^{\dagger}_{m_k'}(\mathbf{r}_\gamma) x_\gamma^2 \mathbf{\Psi}_{m_l}(\mathbf{r}_\gamma) \right) d\mathbf{r}_\gamma \ . \tag{4.14}$$

Again, the first integrand will integrate to zero unless for corresponding coordinates, the m values are equal, in which case the integral will evaluate to unity. In this case

[4] Some constraint on this direction has been made indirectly, through the limiting of the quantum number m to values between zero and N_s inherently cuts the Hilbert space the wavefunctions occupy, and effectively cuts the length of the cylinder.

the m values in the second integrand must be equal, so as to abide by the conserved M (Eq. 4.1).

We must evaluate this second integral in order to determine the matrix elements of confinement. They take the form

$$\begin{aligned}(V_{conf})^{n_1,m_1,p_1}_{n_2,m_2,p_2} &= a\frac{sgn(\sigma')sgn(\sigma)}{N!}\int \left(\mathbf{\Psi}^{\dagger}_{n_1,m_1,p_1}(\mathbf{r})x^2\mathbf{\Psi}_{n_2,m_2,p_2}(\mathbf{r})\right)d\mathbf{r} \\ &= \frac{a}{L}\int\sum_{j=0}^{3}\frac{x^2}{\sqrt{2^{n_1+n_2-2j}(n_1-j)!(n_2-j)!\pi}}\zeta^{*}_{n_1,p_1,j}(z)\zeta_{n_2,p_2,j}(z)e^{-i\frac{2\pi}{L}(m_1-m_2)y} \\ &\times e^{-\frac{1}{2}\left(x-\frac{2\pi m_1}{L}\right)^2-\frac{1}{2}\left(x-\frac{2\pi m_2}{L}\right)^2}H_{n_1-j}\left(x-\frac{2\pi m_1}{L}\right)H_{n_2-j}\left(x-\frac{2\pi m_2}{L}\right)d\mathbf{r}\ . \quad (4.15)\end{aligned}$$

Since we've required that $m_1 = m_2 = m$ we can evaluate the $y-$integral to L, as the integrand is 1, over the domain of integration $y \in [0, L)$. This leaves the $x-$ and $z-$integrals

$$\begin{aligned}(V_{conf})^{n_1,m,p_1}_{n_2,m,p_2} &= \frac{a}{\sqrt{\pi}}\sum_{j=0}^{3}\frac{1}{\sqrt{2^{n_1+n_2-2j}(n_1-j)!(n_2-j)!}}\int_{-w}^{w}\zeta^{*}_{n_1,p_1,j}(z)\zeta_{n_2,p_2,j}(z)dz \\ &\times\int_{-\infty}^{\infty}\left[e^{-\left(x-\frac{2\pi m}{L}\right)^2}x^2H_{n_1-j}\left(x-\frac{2\pi m}{L}\right)H_{n_2-j}\left(x-\frac{2\pi m}{L}\right)\right]dx\ . \quad (4.16)\end{aligned}$$

The $z-$integrals are over the quantum well, and are over an orthogonal set of functions $\zeta_j(z)$, so this integral returns $\delta_{n_1,n_2}\delta_{p_1,p_2}$. We make the change of variable $u = x - \frac{2\pi m}{L}$ and the substitutions for simplicity $\alpha = n_1 - j$, $\beta = n_2 - j$ and our matrix elements become

$$\begin{aligned}(V_{conf})^{n_1,m,p_1}_{n_2,m,p_2} &= \frac{a}{\sqrt{\pi}}\sum_{j=0}^{3}\frac{\delta_{p_1,p_2}}{\sqrt{2^{n_1+n_2-2j}(n_1-j)!(n_2-j)!}} \\ &\times\int_{-\infty}^{\infty}H_\alpha(u)H_\beta(u)\left(u^2+\frac{4\pi m}{L}u+\frac{4\pi^2m^2}{L^2}\right)e^{-u^2}du \\ &= \frac{a}{\sqrt{\pi}}\sum_{j=0}^{3}\frac{\delta_{p_1,p_2}}{\sqrt{2^{n_1+n_2-2j}(n_1-j)!(n_2-j)!}} \\ &\times\int_{-\infty}^{\infty}H_\alpha(u)H_\beta(u)\left(\frac{1}{4}H_2(u)+\frac{1}{2}H_0(u)+\frac{4\pi m}{L}\left(\frac{1}{2}H_1(u)\right)+\frac{4\pi^2m^2}{L^2}\right)e^{-u^2}du\ ,\end{aligned} \quad (4.17)$$

where we have expressed u^2 and u in terms of Hermite polynomials. Since $H_0(u) = 1$, we can consolidate the second and fourth terms within the parentheses in the integrand in Eq. 4.17 and separate the integrals:

$$(V_{conf})^{n_1,m,p_1}_{n_2,m,p_2} = \frac{a}{\sqrt{\pi}} \sum_{j=0}^{3} \frac{\delta_{p_1,p_2}}{\sqrt{2^{n_1+n_2-2j}(n_1-j)!(n_2-j)!}} \left[\frac{1}{4} \int_{-\infty}^{\infty} H_\alpha(u) H_\beta(u) H_2(u) e^{-u^2} du + \frac{2\pi m}{L} \int_{-\infty}^{\infty} H_\alpha(u) H_\beta(u) H_1(u) e^{-u^2} du + \left(\frac{1}{2} + \frac{4\pi^2 m^2}{L^2} \right) \int_{-\infty}^{\infty} H_\alpha(u) H_\beta(u) e^{-u^2} du \right] . \quad (4.18)$$

From Gradshteyn and Ryzhik (1943) Eqn. [7.375.1] [71] we have

$$\int_{-\infty}^{\infty} e^{-x^2} H_k(x) H_m(x) H_n(x) dx = \frac{2^{\frac{m+n+k}{2}} \pi^{1/2} k! m! n!}{(s-k)!(s-m)!(s-n)!} , \quad (4.19)$$

for $2s = m + n + k$ even. For odd $m + n + k$ the integral evaluates to zero. With this formulation our expression in Eq. 4.18 evaluates to

$$(V_{conf})^{n_1,m,p_1}_{n_2,m,p_2} = \frac{a}{\sqrt{\pi}} \sum_{j=0}^{3} \frac{\delta_{p_1,p_2}}{\sqrt{2^{n_1+n_2-2j}(n_1-j)!(n_2-j)!}} \left[\frac{1}{4} \frac{2^{\frac{\alpha+\beta+2}{2}} \sqrt{\pi}\ 2!\ \alpha!\ \beta!}{\left(\frac{\alpha+\beta}{2}-1\right)!\left(\frac{\beta-\alpha}{2}+1\right)!\left(\frac{\alpha-\beta}{2}+1\right)!} + \frac{1}{2} \left(\frac{4\pi m}{L} \right) \frac{2^{\frac{\alpha+\beta+1}{2}} \sqrt{\pi}\ 1!\ \alpha!\ \beta!}{\left(\frac{\alpha+\beta}{2}-\frac{1}{2}\right)!\left(\frac{\beta-\alpha}{2}+\frac{1}{2}\right)!\left(\frac{\alpha-\beta}{2}+\frac{1}{2}\right)!} + \left(\frac{1}{2} + \frac{4\pi^2 m^2}{L^2} \right) \sqrt{\pi}\ 2^\alpha \alpha! \delta_{\alpha,\beta} \right] . \quad (4.20)$$

It must be understood that the first term will be zero unless $\alpha + \beta$ is even, and the second term must be zero unless $\alpha+\beta$ is odd. Thus we have, after some simplification, and resubstituting,

$$(V_{conf})^{n_1,m,p_1}_{n_2,m,p_2} = a\sum_{j=0}^{3} \frac{\delta_{p_1,p_2}}{\sqrt{2^{n_1+n_2-2j}(n_1-j)!(n_2-j)!}}$$
$$\left[\left(\frac{1}{2}+\frac{4\pi^2m^2}{L^2}\right)2^{n_1-j}(n_1-j)!\delta_{n_1,n_2} + 2^{\frac{n_1+n_2-2j-2}{2}}(n_1-j)!(n_2-j)!\right.$$
$$\left.\times\begin{cases}\frac{2}{\left(\frac{n_1+n_2-2j}{2}-1\right)!\left(\frac{n_2-n_1}{2}+1\right)!\left(\frac{n_1-n_2}{2}+1\right)!} & \text{for } n_1+n_2 \text{ even}\\ \frac{4\pi m}{L}\frac{\sqrt{2}}{\left(\frac{n_1+n_2-2j}{2}-\frac{1}{2}\right)!\left(\frac{n_2-n_1}{2}+\frac{1}{2}\right)!\left(\frac{n_1-n_2}{2}+\frac{1}{2}\right)!} & \text{for } n_1+n_2 \text{ odd}\end{cases}\right] \quad (4.21)$$

Applying this term to the diagonal elements of the interaction matrix from Section 4 for each m_i in the diagonal term, we can examine the effect of the imposition of the parabolic confinement on the ground state and gap. FIG. 4.1 shows a gap appearing for several values of the confinement parameter a_{conf}, namely at $a_{conf} \approx 0.07$ (in some units), where we observe a gap of $\Delta E \approx 0.015 E_C$, where E_C is the Coulomb energy (here about 7 meV), thus our gap is on the order of $\Delta E \approx 0.105$ meV, or 1.2 K. It is possible that the reopening gap phenomenon indicates that while the parabolic confinement coefficient is increased or decreased, the energy levels of the parabolic potential begin to move the system out of the condensed FQHE state and into an ungapped state. The system then recondenses at the higher a_{conf} into a higher ν^* state (i.e. transitioning from $\nu = \frac{1}{3}$ to $\frac{2}{5}$ [72]). The wavefunction of the ground state in the region of the large gap ($a_{conf} \approx 0.07$) is confirmed to be in large part similar to the Laughlin-like wavefunction of maximal particle separation, i.e. for $N = 4$ particles as in the calculations for Fig. 4.1, we see maximal occupancy of the $m = 0, 3, 6, 9$ states in a sample with possible occupancy in $m = 0, \ldots, 9$. With both $n = 0, 3$ states present, we see the occupancy being split fairly equally between all possible configurations of two particles in $n = 3$, two particles in $n = 0$.

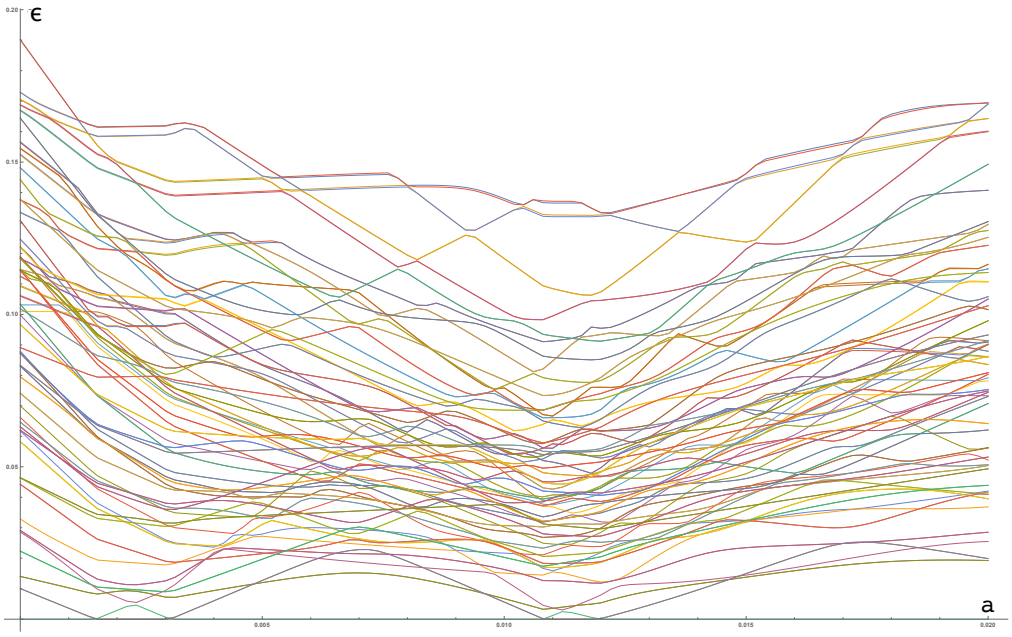

Figure 4.1. Lowest ten energy eigenvalues of the COM basis interaction matrix for $M = 13, \ldots, 23$, with $N = 4$ particles, with parabolic confinement term added on diagonal elements. Gap is absent at $a_{conf} = 0$, then appears with increasing value of the confinement strength. Smaller gap reappears at lower and higher a_{conf}, possibly indicative of other FQHE ground states [72]. Energy scale plotted in units of Coulomb energy $\frac{e^2}{\epsilon l_b}$ which at this field is $E_C \approx 7\ meV$.

5. SUPERCONDUCTIVITY: THE REAL-SPACE BOGOLIUBOV FORMALISM

5.1 The Bogliubov-de Gennes Equations for Superconductivity

Our goal is to introduce a pairing potential via a superconductive proximity effect at some location in our sample, wherein we might observe novel quasiparticle formation. In order to realize this, we must investigate our sample in the context of a superconducting gap, by injecting the Bogoliubov formalism to characterize superconducting excitations. It has been shown in [73] that a normal superconductor can induce a proximity effect in the valence band, thus generating a pair potential for holes in materials like GaAs. The excitations we examine take the familiar form of Cooper pairs made up of hole and antihole pairs within our system.[1] This formalism suggests an effective Hamiltonian in terms of the field operators

$$\begin{aligned} \hat{\Psi}(\mathbf{r},\sigma) &= \sum_{\mathbf{k}} e^{i\mathbf{k}\cdot\mathbf{r}} \hat{a}_{\mathbf{k},\sigma} \\ \hat{\Psi}^{\dagger}(\mathbf{r},\sigma) &= \sum_{\mathbf{k}} e^{-i\mathbf{k}\cdot\mathbf{r}} \hat{a}^{\dagger}_{\mathbf{k},\sigma} \end{aligned} \tag{5.1}$$

where the subscript σ is the spin index, which for electrons can be $\uparrow$ or $\downarrow$, but which in principle for holes can be J_z or $s_z = -\frac{3}{2}, -\frac{1}{2}, \frac{1}{2}, \frac{3}{2}$, or some linear combination therein, which is in fact the case for our system, which finds the two lowest-lying energy states in the $n = 0, 3$ configurations, with $z-$projection of pseudospin $s_{z,n=0} = \frac{3}{2}, s_{z,n=3} \approx -\frac{3}{2}$. We will regard these two energy states as lying considerably farther from the nearest excitations than from one another, especially near their crossing point. The hole creation and annihilation operators for momentum $\mathbf{k}$ and spin σ are $\hat{a}^{\dagger}_{\mathbf{k},\sigma}, \hat{a}_{\mathbf{k},\sigma}$

[1] The derivation in this section draws from Refs. [74, 75], adapted to our system.

($\hat{a}_{\mathbf{k},\sigma}$ may also be thought of as an antihole creation operator), which follow the fermionic anti-commutation relations:

$$\begin{aligned}\left\{\hat{a}^{\dagger}_{\mathbf{k},\sigma}, \hat{a}_{\mathbf{k}',\sigma'}\right\} &= \delta_{\mathbf{k},\mathbf{k}'}\delta_{\sigma,\sigma'} \\ \{\hat{a}_{\mathbf{k},\sigma}, \hat{a}_{\mathbf{k}',\sigma'}\} &= 0 \\ \left\{\hat{a}^{\dagger}_{\mathbf{k},\sigma}, \hat{a}^{\dagger}_{\mathbf{k}',\sigma'}\right\} &= 0\end{aligned} \tag{5.2}$$

The field operators $\hat{\Psi}(\mathbf{r},\sigma), \hat{\Psi}^{\dagger}(\mathbf{r},\sigma)$ thus share the fermionic-like commutation relations, with the added position-space delta-function:

$$\begin{aligned}\left\{\hat{\Psi}(\mathbf{r},\sigma), \hat{\Psi}^{\dagger}(\mathbf{r}',\sigma')\right\} &= \delta_{\sigma,\sigma'}\delta(\mathbf{r}-\mathbf{r}') \\ \left\{\hat{\Psi}(\mathbf{r},\sigma), \hat{\Psi}(\mathbf{r}',\sigma')\right\} &= 0 \\ \left\{\hat{\Psi}^{\dagger}(\mathbf{r},\sigma), \hat{\Psi}^{\dagger}(\mathbf{r}',\sigma')\right\} &= 0\end{aligned} \tag{5.3}$$

In the basis of these field operators we can write the effective Hamiltonian for the system:

$$\mathcal{H}_{eff} = \int \left\{ \sum_{\sigma} \Psi^{\dagger}(\mathbf{r},\sigma)\mathcal{H}_0\Psi(\mathbf{r},\sigma) + \Delta(\mathbf{r})\Psi^{\dagger}(\mathbf{r},\uparrow)\Psi^{\dagger}(\mathbf{r},\downarrow) + \Delta^{*}(\mathbf{r})\Psi(\mathbf{r},\uparrow)\Psi(\mathbf{r},\downarrow) \right\} d\mathbf{r}, \tag{5.4}$$

where $\Delta(\mathbf{r})$ is the number that replaces field operators by their mean-field values $\Delta_k(\mathbf{r}) = V\langle\Psi(\mathbf{r},\uparrow)\Psi(\mathbf{r},\downarrow)\rangle$, and $\mathcal{H}_0$ is the hole energy in magnetic and electric fields discussed previously:

$$\mathcal{H}_0 = \mathcal{H}_L + eE_z(x)z + eE_{x,\sigma}x - \mu + \frac{1}{2}\sum_{i,j}\frac{e^2}{\epsilon|\mathbf{r}_i - \mathbf{r}_j|} \tag{5.5}$$

with the Luttinger hamiltonian $\mathcal{H}_L$, chemical potential μ, the top gate-induced electric field E_z, and the resulting energy-imbalance-created effective electric field in the $x-$direction:

$$E_{x,\sigma} \approx \frac{\Delta\epsilon_{\sigma}}{e\Delta x}, \tag{5.6}$$

where Δx is the approximate distance between the two gated regions (or the gated and ungated region), and $\Delta\epsilon_{\sigma}$ is the energy change that a particle in the spin state σ experiences moving between these regions, which can be tuned using the gate

controlled E_z as in Fig. 2.6. The difference between these energy changes is what gives rise to distinct drift velocities and corresponding shifts in the center of the wavefunctions of the $n = 0, 3$ ground states.

We specifically locate the region in which the two states are degenerate or nearly so, i.e. $\mathcal{H}_L + eE_z(x)z$ values are equal (at the crossing location in Fig. 2.8), and thus in our effective model can be disregarded. The $eE_{x,\sigma}x$ term contributes the amount $eE_{x,\sigma}L\left(k_y - \frac{v_\sigma}{\omega_c}\right)$, where the drift velocity is $v_\sigma = -\frac{cE_{x,\sigma}}{B}$, and the interaction energies can be computationally determined subsequently [76].

We can also determine the value of the mean field pair potential term $\Delta_k(\mathbf{r})$, the term corresponding to which in Eq. 5.4, it should be noted, does not conserve particle number, given that it is the amplitude associated with the introduction of a Cooper pair (or annihilation in the case of the Hermitian conjugate). In our model we will assume that the superconducting gap $\Delta(x, y)$ is not a function of position but can be thought of as a constant, at least in a small region of interest. In that case the term $\Delta_k(\mathbf{r})$ can be written:

$$\begin{aligned}\Delta_k(\mathbf{r}) = V\left\langle\Psi(\mathbf{r},\uparrow)\Psi(\mathbf{r},\downarrow)\right\rangle &= V\Delta\int\Psi_0(\mathbf{r})\Psi_3(\mathbf{r})d\mathbf{r} \\ &= V\Delta\int_{-\frac{w}{2}}^{\frac{w}{2}}\zeta_{n=0,p=0}(z)\zeta_{n=3,p=0}(z)dz \\ &\quad\times\frac{1}{\sqrt{48}}\left(2k_y - \frac{1}{\omega_c}(v_0 - v_3)\right)^3 e^{-\left(2k_y - \frac{1}{\omega_c}(v_0-v_3)\right)^2/4} \quad (5.7)\end{aligned}$$

If we remove the volume prefactor and isolate the $k_y = 0$ term, what remains is

$$\Delta_k(\mathbf{r}) = \frac{\Delta}{4\sqrt{3}}\left(\frac{v_3 - v_0}{\omega_c}\right)^3 e^{-\left(\frac{v_3-v_0}{2\omega_c}\right)^2}\int_{-\frac{w}{2}}^{\frac{w}{2}}\zeta_{n=0,p=0}(z)\zeta_{n=3,p=0}(z)dz, \quad (5.8)$$

where the $z-$integral must be performed numerically over the envelope wavefunctions in the $z-$direction. The quantum number n refers to the Landau Level index of the hole wavefunction, and the $p = 0, 1, 2, 3$ quantum number indexes the four-vector of the individual solution.

For our purposes we must utilize pseudospin-dependent Bogoliubov-de Gennes (B-dG) equations, since the two states we consider have different energies $\mathcal{H}_0$ due to

the different effective electric fields E_x they experience in the $x-$direction due to the gradient of the two states' energies as a function of the spatial variable that spans the direction perpendicular to the boundary between the different E_z-field regions (Eq. 5.6). This leads us to search for new quasiparticle operators which will replace the hole/antihole creation and annihilation operators. These new quasiparticles will serve to diagonalize the effective Hamiltonian in Eq. 5.4 [74,75]. These new operators take the form (from [74])

$$\begin{aligned}\hat{\Psi}(\mathbf{r}\uparrow) &= \sum_n \left(\gamma_{n\uparrow} u_n(\mathbf{r}) - \gamma^\dagger_{n\downarrow} v^*_n(\mathbf{r})\right) \\ \hat{\Psi}(\mathbf{r}\downarrow) &= \sum_n \left(\gamma_{n\downarrow} u_n(\mathbf{r}) - \gamma^\dagger_{n\uparrow} v^*_n(\mathbf{r})\right),\end{aligned} \tag{5.9}$$

where the new $\gamma_n^{(\dagger)}$ operators create quasiparticle excitations in some state n, which we will take to be indexed by our pseudospin $n = 0, 3$ or $\uparrow, \downarrow$. In the basis of these "position-dependent eigenfunctions" $u_{\uparrow/\downarrow}(\mathbf{r})$ and $v_{\uparrow/\downarrow}(\mathbf{r})$, we can write our Bogoliubov-de Gennes equations with pseudospin-indexing subscripts. These $u_{\uparrow/\downarrow}(\mathbf{r})$ and $v_{\uparrow/\downarrow}(\mathbf{r})$ are a position-space analogy of the momentum space u_k and v_k from the BCS theory, which are coefficients of Cooper pair creation and vacuum terms in the BCS wavefunction, respectively.

$$\begin{aligned}\epsilon u_\uparrow(\mathbf{r}) &= \mathcal{H}_{0,\uparrow} u_\uparrow(\mathbf{r}) + \Delta_k(\mathbf{r}) v_\uparrow(\mathbf{r}) \\ \epsilon v_\uparrow(\mathbf{r}) &= -\mathcal{H}_{0,\uparrow} v_\uparrow(\mathbf{r}) + \Delta^*_k(\mathbf{r}) u_\uparrow(\mathbf{r}) \\ \epsilon u_\downarrow(\mathbf{r}) &= \mathcal{H}_{0,\downarrow} u_\downarrow(\mathbf{r}) + \Delta_k(\mathbf{r}) v_\downarrow(\mathbf{r}) \\ \epsilon v_\downarrow(\mathbf{r}) &= -\mathcal{H}_{0,\downarrow} v_\downarrow(\mathbf{r}) + \Delta^*_k(\mathbf{r}) u_\downarrow(\mathbf{r}),\end{aligned} \tag{5.10}$$

Our equations can be written in a matrix form as

$$\begin{pmatrix} \mathcal{H}_{0,\uparrow} & 0 & \Delta_k & 0 \\ 0 & \mathcal{H}_{0,\downarrow} & 0 & \Delta_k \\ \Delta^*_k & 0 & -\mathcal{H}_{0,\uparrow} & 0 \\ 0 & \Delta^*_k & 0 & -\mathcal{H}_{0,\downarrow} \end{pmatrix} \begin{pmatrix} u_\uparrow \\ u_\downarrow \\ v_\uparrow \\ v_\downarrow \end{pmatrix} = \epsilon \begin{pmatrix} u_\uparrow \\ u_\downarrow \\ v_\uparrow \\ v_\downarrow \end{pmatrix}, \tag{5.11}$$

which has solutions

$$\begin{aligned}\epsilon_{\uparrow,\pm} &= \pm\sqrt{\left(\mathcal{H}_{0,\uparrow}\right)^2 + \left|\Delta_k\right|^2} \\ \epsilon_{\downarrow,\pm} &= \pm\sqrt{\left(\mathcal{H}_{0,\downarrow}\right)^2 + \left|\Delta_k\right|^2}\end{aligned} \tag{5.12}$$

with corresponding amplitudes

$$\begin{pmatrix} u_\uparrow \\ u_\downarrow \\ v_\uparrow \\ v_\downarrow \end{pmatrix} = \begin{pmatrix} \frac{\mathcal{H}_{0,\uparrow}\pm\sqrt{\left(\mathcal{H}_{0,\uparrow}\right)^2+\left|\Delta_k\right|^2}}{\Delta_k^*} \\ 0 \\ 1 \\ 0 \end{pmatrix}, \begin{pmatrix} 0 \\ \frac{\mathcal{H}_{0,\downarrow}\pm\sqrt{\left(\mathcal{H}_{0,\downarrow}\right)^2+\left|\Delta_k\right|^2}}{\Delta_k^*} \\ 0 \\ 1 \end{pmatrix}, \tag{5.13}$$

respectively, which might be thought of as the linear combinations that give rise to our quasiparticle excitations.

Our self-consistent treatment within this formalism shows that the single-particle energies as well as interaction effects can be taken into account when determining the value of Δ_k for our system, and that the quasiparticle energies $\epsilon_{\uparrow/\downarrow,\pm}$ of our system might introduce a gap in proper conditions. We will consider various values of Δ_k for our final results, in order to monitor for the vanishing and reintroduction of the gap parameter as a function of the superconducting gap energy, i.e. tuning the $\epsilon_{\uparrow/\downarrow,\pm}$ levels in a region close to the Fermi level [17].

5.2 Inducing Superconductivity on a Pseudospin-Separated Fractional Quantum Hall State

Interest and investigation into hybrid quantum Hall effect and superconducting systems began in the early 1990s, when proximity superconducting coupling to integer quantum Hall edges was considered in [77, 78]. Our goal here is to investigate proximity effects in Fractional quantum Hall state of holes. Given that we have shown evidence for possible co-propagating edge states in a sample between gated and ungated regions in this section, it is clear that the relative velocities $(v_3 - v_0)$ make up a portion of the Δ_k term (Eq. 5.8). Modifying our system for computational simplicity

is merely a matter of modifying this relative velocity term, and given the freedom to manipulate the Δ_k term that we will later take, this modification is likely not deleterious to our result. With that said, we will eschew the structure of our system, half in no external electric field, half gated as given by Fig. 2.6, in favor of a simpler energetic structure that will benefit our interaction calculations, given by Fig. 5.1.

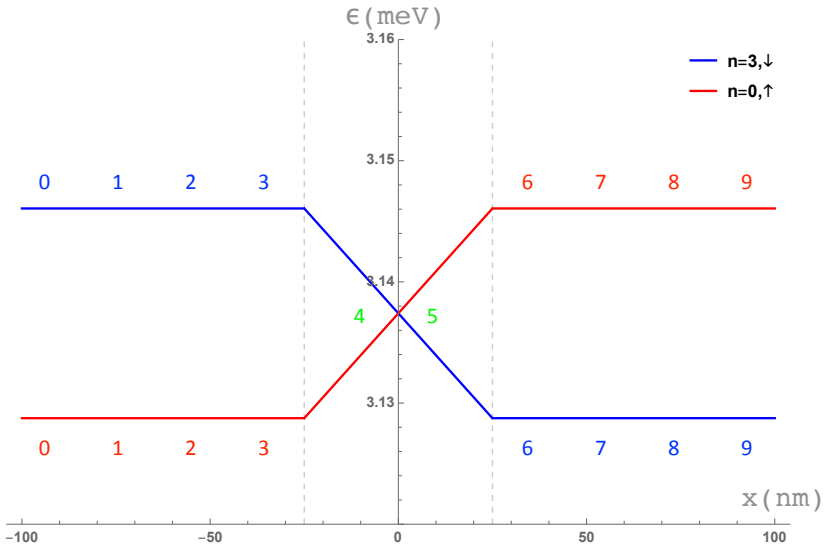

Figure 5.1. Ground state crossing in a synthetic symmetric system, where energy splitting between ↑ and ↓ states is of the same order as that created in $E_z = 0$ or $E_z = 6\frac{kV}{cm}$.

In order to shift our system of interacting holes on a cylinder into one in which we might induce a superconductivity effect, we choose a sample number of particles to start. In this work we begin with $N = 4$ holes, and we set up our system's parameters in such a way that it should be in the $\nu = \frac{1}{3}$ FQHE state with the given applied magnetic field and particle density (see Section 3.1). For our system we have chosen our magnetic field value to be $B_z = 2.55\ T$, our quantum well width is 200 $\mathring{A}$, and the "right" half of our system is under an externally applied gate-controlled DC electric field of $E_z = 6\frac{kV}{cm}$. With these considerations in mind, our cyclotron energy is $\hbar\omega_c \approx 0.3\ meV$, and our Coulomb energy is on the order of $\frac{e^2}{\epsilon l_B} \approx 7\ meV$.

If we assume that we might neglect the upper branches of Fig. 5.1, we may form a curated basis in the configuration-interaction scheme in which the available states for $N = 4$ particles have momentum quantum numbers $m_i = 0, \ldots, 9$, where $m \in [0, 3]$ may only be $\uparrow$, $m \in [6, 9]$ may only be $\downarrow$, but due to the near-degeneracy in the center of our sample, $m = 4, 5$ may be both $\uparrow$ and $\downarrow$. To simulate the crossing we put a small energy tax for particles to occupy the $m = 4, 5$ states, we do not allow the upper branches' states to be part of our basis for simplicity's sake, and then we allow the particles within this new basis to interact, and we numerically calculate the energies and wavefunctions in the same basis and with the same methods as in Section 4.2, with the caveat that the wavefunctions used for the $n = 3$ states used to calculate the pseudopotentials should be those with the external gate field E_z applied (see Fig. 2.3), but those in the $n = 0$ state should be in $E_z = 0$.

Our first goal is to recover a Laughlin-like ground state of maximal particle separation in our system to show that the system remains in the FQHE ground state even under these modified conditions for specifically four particles, and we apparently do, as shown in Fig. 5.2. We are reassured that the ground state near $a_{conf} \approx 0.05$, at the location of the largest gap, recovers the character of the Laughlin-like repulsion, with particles principally occupying states $(\sigma, m) = (\uparrow, 0), (\uparrow, 3), (\downarrow, 6), (\downarrow, 9)$. Now that we have demonstrated this particular ground state, we will relax the particle number conservation on our system, and calculate the Coulomb interaction energies of $N = 2, 6$ hole states. That said, these states will be calculated with all parameters from the $N = 4$ hole state. The reason we choose these particular numbers is that once we introduce superconductivity via some simulation of a proximity effect into our system, the system must be able to move between states with more or fewer Cooper pairs, provided the energy cost Δ_k is paid (See Eq. 5.4). To that effect we have calculated the interaction energies of our system with these higher and lower occupancy states, as shown in Figs. 5.3 and 5.4.

The systems' lowest lying states' wavefunctions can then be joined into a new basis in which we will begin to diagonalize our Bogoliubov-de Gennes effective Hamiltonian

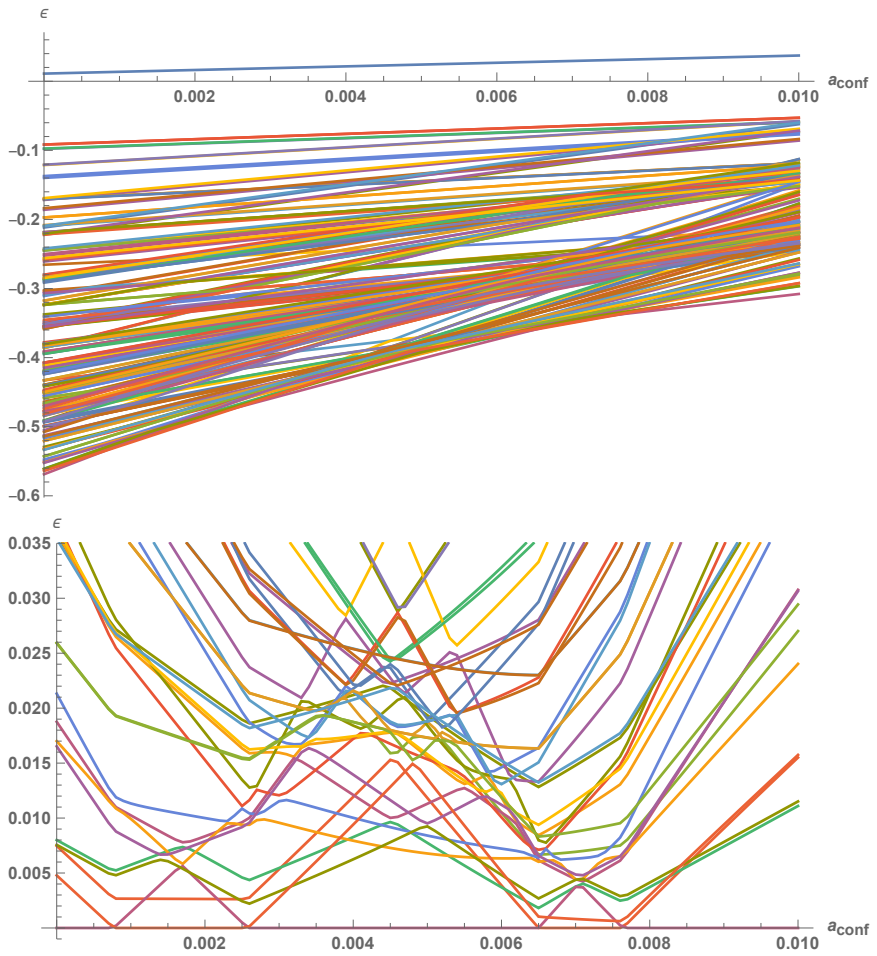

Figure 5.2. (top) Diagonalized Coulomb interaction matrix in curated basis, with crossing simulated in center of sample, and spins selectively populating the left (↑) and right (↓) (bottom) Same, with lowest lying states shown in greater detail, after setting lowest state to $\epsilon = 0$. Energies shown in units of Coulomb energy.

(again, Eq. 5.4) ground states, which must be set to similar energy ranges by subtracting the a charging energy proportional to N_{avg}^2, where N_{avg} is the average particle occupancy for a certain state. The basis states that we have created are normalized linear combinations of $N = 2, 4$, or 6 particle states, taking the general form

$$\Psi_N(\mathbf{r}_1, \mathbf{r}_2, \ldots, \mathbf{r}_N) = \sum_i c_{m_{i,1}, m_{i,2}, \ldots, m_{i,N}} \mathcal{A}\left[\psi_{m_{i,1}}(\mathbf{r}_1)\psi_{m_{i,2}}(\mathbf{r}_2)\cdots\psi_{m_{i,N}}(\mathbf{r}_N)\right], \quad (5.14)$$

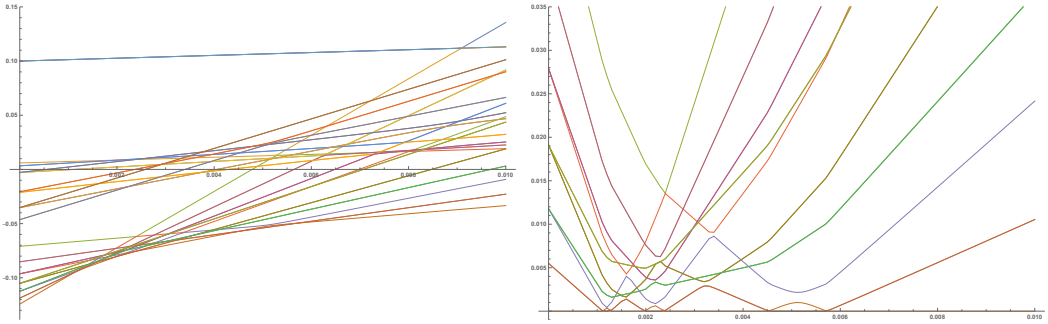

Figure 5.3. Same as Fig. 5.2 but with $N = 2$ holes instead of 4.

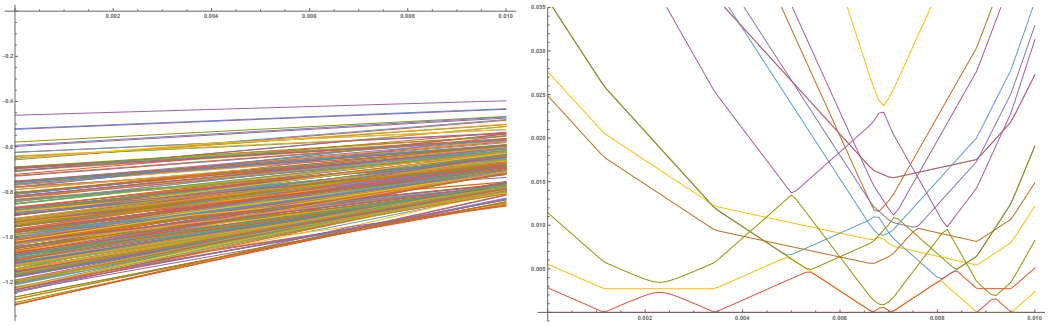

Figure 5.4. Same as Fig. 5.2 but with $N = 6$ holes instead of 4.

where $\mathcal{A}$ is the antisymmetrization operator, acting on the single particle states $\psi_m(\mathbf{r})$ (essentially forming a Slater determinant, as shown in Eq. 4.5), and we can associate $|c_{m_{i,1},m_{i,2},\ldots,m_{i,N}}|^2$ with the probability of finding our system in the N particle state identified with that particular set of $\{m_i\}$ occupation numbers. The introduction of superconductivity into this state requires that we introduce Cooper pair creation and annihilation operators $\Delta_k \Psi^\dagger(\mathbf{r},\uparrow)\Psi^\dagger(\mathbf{r},\downarrow)$, $\Delta_k^* \Psi(\mathbf{r},\uparrow)\Psi(\mathbf{r},\downarrow)$, as defined in Eq. 5.1. Practically speaking, this amounts to off-diagonal terms in the Bogoliubov-de Gennes Hamiltonian between $N, N-2$ or $N, N+2$ states.

We limit the creation of Cooper pairs to states near the crossing region in our system, simulating a short-range proximity effect of a superconducting wire placed in the region directly next to the top-gated region, so that only Cooper pairs with combina-

tions of states $(\sigma_1, m_1; \sigma_2, m_2) = (\uparrow, 4; \downarrow, 5), (\uparrow, 5; \downarrow, 4), (\uparrow, 3; \downarrow, 5), (\uparrow, 4; \downarrow, 6), (\uparrow, 3; \downarrow, 6)$ are physically realized. The Cooper pair creation amplitude is manually tuned to be largest for the $m = 4, 5$ Cooper pair states, presuming that the creation amplitudes are smaller for more spatially separated states. We additionally add in a tunneling amplitude for states with particles near the crossing point to be able to move into the crossing region or all the way from one side of the system to the other, allowing the pseudospin species to mix, and via their mixing create the quasiparticle excitations we hope to observe. In addition to this consideration we subtract from our basis states' Coulomb interaction energies ($\mathcal{H}_0$) the charging energy associated with the average number of particles in the individual states, proportional to N^2. Charging the diagonal term in the Hamiltonian has been similarly introduced in treatments of superconductivity in finite-size electron systems [33, 79]. We choose to place the Fermi energy or chemical potential μ in the neighborhood of some state, chosen arbitrarily to be one of the $N = 2$ states (arbitrary because we are in effect subtracting a constant factor from the diagonal of our Hamiltonian). With these considerations, our numerical calculations allow us to extract the eigenenergies of the Bogoliubov-de Gennes Hamiltonian for a variety of values of Δ_k, the superconducting gap parameter, and locate a gapped energy spectrum in the region of our FQHE ground state where the states are degenerate near the bottom of the gap, and enter the gap to close it in the region of the critical value of Δ_k, as shown in Fig. 5.5 [28, 33, 35].

Within Fig. 5.5 we see four degenerate states near the center of the gap at $\Delta_k \approx 1.5E_C$, and two other states that enter the gap quite separately at larger Δ_k, so we investigate the effects of increasing the tunneling parameter (see Fig. 5.6), where we observe an anticrossing between these groups of states. While at present stage the exact proof that these are parafermions, which requires numerical simulation of the fractional Josephson effect, and much bigger number of particles, is not available, Fig. 5.6 clearly demonstrates a connection of these mid-gap states. Furthermore, significant change of tunneling does not affect energies of these states, which continue to be in the middle of the gap, indicating a topologically non-trivial state, i.e. one that

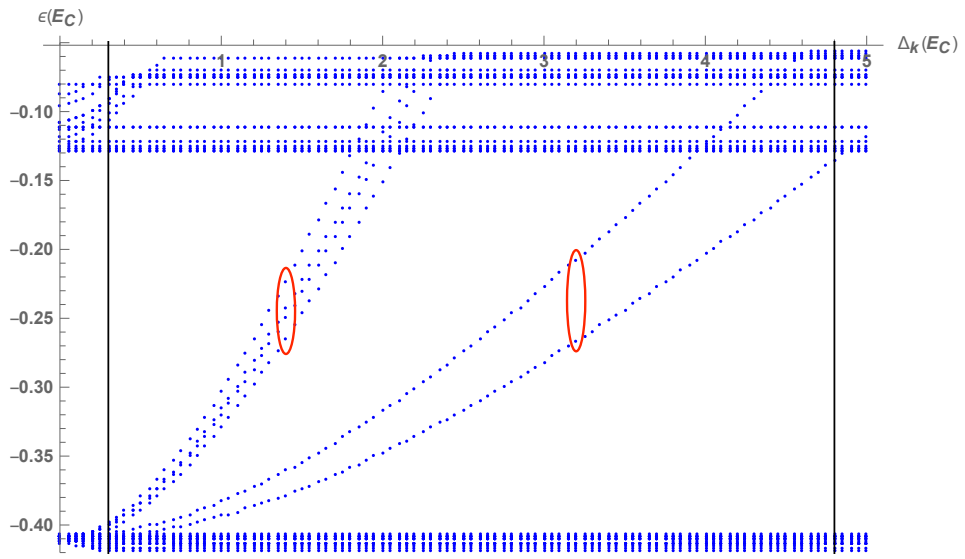

Figure 5.5. Energy plotted in units of Coulomb energy as a function of Δ_k values in units of Coulomb energy. Gap at low values of Δ_k can be seen closing between the vertical lines, then reopening at higher values of Δ_k. This indicates a critical Δ_k, as discussed in [17] in the region of $\Delta_k \approx 0.4 - 4.8E_C \approx 3 - 34\ meV$. Degenerate states enter the gap near this critical Δ_k, and also near higher Δ_k where only two states enter gap, indicated by red circles.

is robust under changes in Δ_k. In addition, repulsion (anticrossing) of these states can be interpreted, similar to repulsion between Majorana zero modes in numerical simulation of Marorana fermions [23].

The three-fold degeneracy of in-gap states we observe in Fig. 5.6 near $\Delta_k \approx 3.5E_C$ seem to repel one another, forming anticrossings, indicating a connection between them, as such a sign of the six-fold degeneracy shown in [79] and [33]. Of note, systems with different topologies may differ in the number of degenerate states that appear to close the gap [69]. In this region within the gap, quasiparticle creation and annihilation does not cost energy, given that the states are degenerate at $\epsilon = 0$, but they are topologically protected from decay into other particles by their separation from the top and bottom of the superconducting gap [35]. We also expect that in the limit as the particle number N is increased toward the thermodynamic limit that the

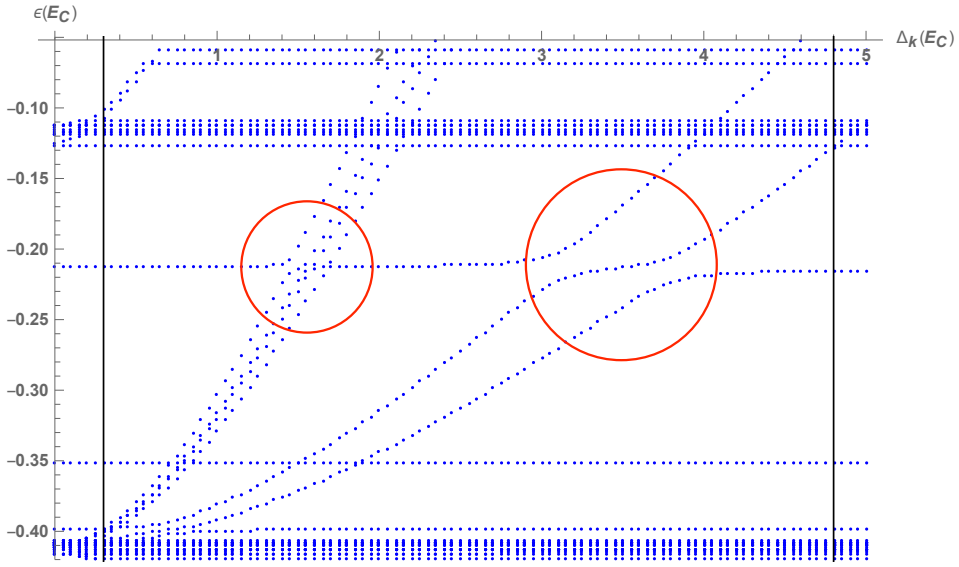

Figure 5.6. Energy plotted in units of Coulomb energy as a function of Δ_k values in units of Coulomb energy, with increased tunneling parameter compared to Fig. 5.5. Anticrossings and robust state at center of gap indicate desired connections between degenerate mid-gap states (red circles).

expression of this degeneracy becomes more pronounced. This result underlines our claim of this platform's support for the detection of parafermion states, and serves to demonstrate the fairly robust experimental setup to realize this, with magnetic fields in the $B_z \approx 2.5\ T$ range, gate controlled electric field of $E_z = 6\frac{kV}{cm}$, resulting in superconducting gap parameters in the low meV energy range.

6. SUMMARY AND CONCLUSIONS

In this work we have established evidence of a new physically realistic parafermion-supporting platform in a two-dimensional hole liquid in Gallium Arsenide. We discussed the single particle phenomena which lead to a spin transition within the ground state of the hole system, modeled by the Γ_8 Luttinger Hamiltonian, which we then manipulated using gate-controlled DC electric fields in order to inlay our system with a strong intrinsic spin-orbit effect. We used this system to numerically create many-body interaction effects using physically realistic pseudopotential calculations, while maintaining the system's FQHE state therein.

After this, we utilized a proximity effect-induced pair production potential to create a superconducting gap, which showed evidence of parafermionic energy signatures in the closing and reopening gap as a function of the superconducting gap parameter Δ_k, where the particles traversing the gap at certain values of the parameter are identified as an onset of six-fold degenerate parafermion states. Spectra allow identification of anticrossings between these states, similar to repulsion of Majorana zero modes in quantum wires. The mid-gap states experience almost no changes in a sizable interval of tunneling amplitudes, and thereby show signatures of topological protection. These states are well-separated from states on either side of the gap. The consequences of this theoretical realization are promising toward future experimental detection and utilization of parafermions in hole systems. In the future, a more computationally exhaustive analysis of the system's properties under interference of the gapped particles would serve as incontrovertible evidence of the parafermion state, but a significantly higher particle number would certainly be necessary for this type of analysis.

Future experimentation may be centered upon braiding operations upon these hole-crossing-based parafermion systems in order to probe the quantum operations

the system is capable of realizing, [80] e.g. the twisted-line junction in [81], or the bilayer schematic with interlayer tunneling in [35]. These braiding operations produce excitations called "genons", which may have a rich class of quantum operations to be realized. It could also be useful to manipulate the system using an in-plane magnetic field, which could manipulate transitions within our system by both modifying the topological nature of the system as well as by directly manipulating the spin-dependent spectrum [40, 82]. Further on, a two-dimensional array of parafermions may generate Fibonacci anyon quasiparticles with universal braiding statistics [19,36].

REFERENCES

[1] P. W. Shor. Fault-tolerant quantum computation. In *Proceedings of 37th Conference on Foundations of Computer Science*, pages 56–65, Oct 1996.

[2] Michael H. Freedman. P/np, and the quantum field computer. *Proceedings of the National Academy of Sciences*, 95(1):98–101, 1998.

[3] A Yu Kitaev. Unpaired Majorana fermions in quantum wires. *Physics-Uspekhi*, 44(10S):131, 2001.

[4] Michael H. Freedman, Michael J. Larsen, and Zhenghan Wang. The two-eigenvalue problem and density of jones representation of braid groups. *Communications in Mathematical Physics*, 228:177–199, June 2002.

[5] D. A. Ivanov. Non-Abelian statistics of half-quantum vortices in p-wave superconductors. *Phys. Rev. Lett.*, 86:268–271, Jan 2001.

[6] A.Yu. Kitaev. Fault-tolerant quantum computation by anyons. *Annals of Physics*, 303(1):2 – 30, 2003.

[7] Chetan Nayak, Steven H. Simon, Ady Stern, Michael Freedman, and Sankar Das Sarma. Non-Abelian anyons and topological quantum computation. *Rev. Mod. Phys.*, 80:1083–1159, Sep 2008.

[8] Gregory Moore and Nicholas Read. Nonabelions in the fractional quantum Hall effect. *Nuclear Physics B*, 360(2):362 – 396, 1991.

[9] Sergey Bravyi. Universal quantum computation with the $\nu = 5/2$ fractional quantum Hall state. *Phys. Rev. A*, 73:042313, Apr 2006.

[10] N. Read and Dmitry Green. Paired states of fermions in two dimensions with breaking of parity and time-reversal symmetries and the fractional quantum Hall effect. *Phys. Rev. B*, 61:10267–10297, Apr 2000.

[11] Ady Stern and Bertrand I. Halperin. Proposed experiments to probe the non-Abelian $\nu = 5/2$ quantum Hall state. *Phys. Rev. Lett.*, 96:016802, Jan 2006.

[12] D. E. Feldman and Alexei Kitaev. Detecting non-Abelian statistics with an electronic Mach-Zehnder interferometer. *Phys. Rev. Lett.*, 97:186803, Nov 2006.

[13] R L Willett, L N Pfeiffer, and West K W. Measurement of filling factor 5/2 quasiparticle interference with observation of charge e/4 and e/2 period oscillations. *Proceedings of the National Academy of Sciences*, 106(22):8853–8858, 2009.

[14] N. Read and E. Rezayi. Beyond paired quantum Hall states: Parafermions and incompressible states in the first excited Landau level. *Phys. Rev. B*, 59:8084–8092, Mar 1999.

[15] Roman M. Lutchyn, Jay D. Sau, and S. Das Sarma. Majorana fermions and a topological phase transition in semiconductor-superconductor heterostructures. *Phys. Rev. Lett.*, 105:077001, Aug 2010.

[16] Yuval Oreg, Gil Refael, and Felix von Oppen. Helical liquids and Majorana bound states in quantum wires. *Phys. Rev. Lett.*, 105:177002, Oct 2010.

[17] S. Tewari, J. D. Sau, and S. Das Sarma. A theorem for the existence of Majorana fermion modes in spin–orbit-coupled semiconductors. *Annals of Physics*, 325(1):219 – 231, 2010. January 2010 Special Issue.

[18] Jason Alicea. Majorana fermions in a tunable semiconductor device. *Phys. Rev. B*, 81:125318, Mar 2010.

[19] Jason Alicea, Yuval Oreg, Gil Refael, Felix von Oppen, and Matthew P. A. Fisher. Non-Abelian statistics and topological quantum information processing in 1d wire networks. *Nature Physics*, 7:412, 2011.

[20] M. Baraban, N. E. Bonesteel, and S. H. Simon. Resources required for topological quantum factoring. *Phys. Rev. A*, 81:062317, Jun 2010.

[21] G Baskaran. Why is Sr2RuO4 not a high Tc superconductor? Electron correlation, Hund's coupling and p-wave instability. *Physica B: Condensed Matter*, 223-224:490 – 495, 1996. Proceedings of the International Conference on Strongly Correlated Electron Systems.

[22] Maissam Barkeshli. Charge $2e/3$ superconductivity and topological degeneracies without localized zero modes in bilayer fractional quantum Hall states. *Phys. Rev. Lett.*, 117:096803, Aug 2016.

[23] Leonid P. Rokhinson, Xinyu Liu, and Jacek K. Furdyna. The fractional a.c. Josephson effect in a semiconductor–superconductor nanowire as a signature of Majorana particles. *Nature Physics*, 8:795 EP –, 09 2012.

[24] V. Mourik, K. Zuo, S. M. Frolov, S. R. Plissard, E. P. A. M. Bakkers, and L. P. Kouwenhoven. Signatures of majorana fermions in hybrid superconductor-semiconductor nanowire devices. *Science*, 336(6084):1003–1007, 2012.

[25] Anindya Das, Yuval Ronen, Yonatan Most, Yuval Oreg, Moty Heiblum, and Hadas Shtrikman. Zero-bias peaks and splitting in an Al-InAs nanowire topological superconductor as a signature of Majorana fermionss nanowire topological superconductor as a signature of Majorana fermions. *Nature Physics*, 8:887, Nov 2012. Article.

[26] Fabrizio Nichele, Asbjørn C. C. Drachmann, Alexander M. Whiticar, Eoin C. T. O'Farrell, Henri J. Suominen, Antonio Fornieri, Tian Wang, Geoffrey C. Gardner, Candice Thomas, Anthony T. Hatke, Peter Krogstrup, Michael J. Manfra, Karsten Flensberg, and Charles M. Marcus. Scaling of majorana zero-bias conductance peaks. *Phys. Rev. Lett.*, 119:136803, Sep 2017.

[27] G. Simion, A. Kazakov, L. P. Rokhinson, T. Wojtowicz, and Y. B. Lyanda-Geller. Impurity-generated non-Abelions. *Phys. Rev. B*, 97:245107, Jun 2018.

[28] David J. Clarke, Jason Alicea, and Kirill Shtengel. Exotic non-Abelian anyons from conventional fractional quantum Hall states. *Nature Communications*, 4(1348), 01 2013.

[29] Jingcheng Liang and Yuli Lyanda-Geller. Charge carrier holes and Majorana fermions. *Phys. Rev. B*, 95:201404, May 2017.

[30] Tailung Wu, Zhong Wan, Aleksandr Kazakov, Ying Wang, George Simion, Jingcheng Liang, Kenneth W. West, Kirk Baldwin, Loren N. Pfeiffer, Yuli Lyanda-Geller, and Leonid P. Rokhinson. Formation of helical domain walls in the fractional quantum Hall regime as a step toward realization of high-order non-Abelian excitations. *Phys. Rev. B*, 97:245304, Jun 2018.

[31] Liang Fu and C. L. Kane. Superconducting proximity effect and Majorana fermions at the surface of a topological insulator. *Phys. Rev. Lett.*, 100:096407, Mar 2008.

[32] J. Wiedenmann, E. Bocquillon, R. S. Deacon, S. Hartinger, O. Herrmann, T. M. Klapwijk, L. Maier, C. Ames, C. Brüne, C. Gould, A. Oiwa, K. Ishibashi, S. Tarucha, H. Buhmann, and L. W. Molenkamp. 4π-periodic Josephson supercurrent in HgTe-based topological Josephson junctions. *Nature Communications*, 7(10303), Jan 2016.

[33] J. Liang, G. E. Simion, and Y. B. Lyanda-Geller. Parafermions, induced edge states and domain walls in the fractional quantum Hall effect spin transitions. arXiv:1904.04719, 2019.

[34] Paul Fendley. Parafermionic edge zero modes in Z_n-invariant spin chains. *Journal of Statistical Mechanics: Theory and Experiment*, 2012(11):P11020, nov 2012.

[35] Jason Alicea and Paul Fendley. Topological phases with parafermions: Theory and blueprints. *Annual Review of Condensed Matter Physics*, 7(1):119–139, 2016.

[36] Roger S. K. Mong, David J. Clarke, Jason Alicea, Netanel H. Lindner, Paul Fendley, Chetan Nayak, Yuval Oreg, Ady Stern, Erez Berg, Kirill Shtengel, and Matthew P. A. Fisher. Universal topological quantum computation from a superconductor-Abelian quantum Hall heterostructure. *Phys. Rev. X*, 4:011036, Mar 2014.

[37] J. P. Eisenstein, H. L. Störmer, V. Narayanamurti, A. C. Gossard, and W. Wiegmann. Effect of inversion symmetry on the band structure of semiconductor heterostructures. *Phys. Rev. Lett.*, 53:2579–2582, Dec 1984.

[38] Yang Liu, A. L. Graninger, S. Hasdemir, M. Shayegan, L. N. Pfeiffer, K. W. West, K. W. Baldwin, and R. Winkler. Fractional quantum Hall effect at $\nu = 1/2$ in hole systems confined to gaas quantum wells. *Phys. Rev. Lett.*, 112:046804, Jan 2014.

[39] Yang Liu, S. Hasdemir, D. Kamburov, A. L. Graninger, M. Shayegan, L. N. Pfeiffer, K. W. West, K. W. Baldwin, and R. Winkler. Even-denominator fractional quantum Hall effect at a Landau level crossing. *Phys. Rev. B*, 89:165313, Apr 2014.

[40] S. Hasdemir, Yang Liu, H. Deng, M. Shayegan, L. N. Pfeiffer, K. W. West, K. W. Baldwin, and R. Winkler. $\nu = 1/2$ fractional quantum hall effect in tilted magnetic fields. *Phys. Rev. B*, 91:045113, Jan 2015.

[41] J. P. Eisenstein, G. S. Boebinger, L. N. Pfeiffer, K. W. West, and Song He. New fractional quantum Hall state in double-layer two-dimensional electron systems. *Phys. Rev. Lett.*, 68:1383–1386, Mar 1992.

[42] Y. W. Suen, L. W. Engel, M. B. Santos, M. Shayegan, and D. C. Tsui. Observation of a ν=1/2 fractional quantum Hall state in a double-layer electron system. *Phys. Rev. Lett.*, 68:1379–1382, Mar 1992.

[43] Aleksandr Kazakov, George Simion, Yuli Lyanda-Geller, Valery Kolkovsky, Zbigniew Adamus, Grzegorz Karczewski, Tomasz Wojtowicz, and Leonid P. Rokhinson. Electrostatic control of quantum Hall ferromagnetic transition: A step toward reconfigurable network of helical channels. *Phys. Rev. B*, 94:075309, Aug 2016.

[44] J. M. Luttinger. Quantum theory of cyclotron resonance in semiconductors: General theory. *Phys. Rev.*, 102:1030–1041, May 1956.

[45] G. E. Simion and Y. B. Lyanda-Geller. Magnetic field spectral crossings of Luttinger holes in quantum wells. *Phys. Rev. B*, 90:195410, Nov 2014.

[46] J. M. Luttinger and W. Kohn. Motion of electrons and holes in perturbed periodic fields. *Phys. Rev.*, 97:869–883, Feb 1955.

[47] J. M. Luttinger. The effect of a magnetic field on electrons in a periodic potential. *Phys. Rev.*, 84:814–817, Nov 1951.

[48] SS Nedorezov. Space quantization in semiconductor films. *Soviet physics, Solid state.*, 12(8):1814–1819, 1971.

[49] Daniel P. Arovas and Yuli Lyanda-Geller. Non-Abelian geometric phases and conductance of spin-$\frac{3}{2}$ holes. *Phys. Rev. B*, 57:12302–12305, May 1998.

[50] Denis V. Bulaev and Daniel Loss. Electric dipole spin resonance for heavy holes in quantum dots. *Phys. Rev. Lett.*, 98:097202, Feb 2007.

[51] Y. B. Lyanda-Geller, T. L. Reinecke, and M. Bayer. Exciton fine structure in coupled quantum dots. *Phys. Rev. B*, 69:161308, Apr 2004.

[52] D. Csontos, P. Brusheim, U. Zülicke, and H. Q. Xu. Spin-$\frac{3}{2}$ physics of semiconductor hole nanowires: Valence-band mixing and tunable interplay between bulk-material and orbital bound-state spin splittings. *Phys. Rev. B*, 79:155323, Apr 2009.

[53] B. Andrei Bernevig and Shou-Cheng Zhang. Intrinsic spin Hall effect in the two-dimensional hole gas. *Phys. Rev. Lett.*, 95:016801, Jun 2005.

[54] Li Mao, Ming Gong, E. Dumitrescu, Sumanta Tewari, and Chuanwei Zhang. Hole-doped semiconductor nanowire on top of an s-wave superconductor: A new and experimentally accessible system for Majorana fermions. *Phys. Rev. Lett.*, 108:177001, Apr 2012.

[55] Aleksandr Kazakov, George Simion, Yuli Lyanda-Geller, Valery Kolkovsky, Zbigniew Adamus, Grzegorz Karczewski, Tomasz Wojtowicz, and Leonid P. Rokhinson. Mesoscopic transport in electrostatically defined spin-full channels in quantum Hall ferromagnets. *Phys. Rev. Lett.*, 119:046803, Jul 2017.

[56] S.-R. Eric Yang, D. A. Broido, and L. J. Sham. Holes at GaAs-$Al_xGa_{1-x}As$ heterojunctions in magnetic fields. *Phys. Rev. B*, 32:6630–6633, Nov 1985.

[57] D. A. Broido and L. J. Sham. Effective masses of holes at GaAs-AlGaAs heterojunctions. *Phys. Rev. B*, 31:888–892, Jan 1985.

[58] L.J. Sham. Theory of valence subbands in GaAs heterostructures. *Surface Science*, 174(1):105 – 110, 1986.

[59] F. D. M. Haldane. Fractional quantization of the Hall effect: A hierarchy of incompressible quantum fluid states. *Phys. Rev. Lett.*, 51:605–608, Aug 1983.

[60] R. B. Laughlin. Anomalous quantum Hall effect: An incompressible quantum fluid with fractionally charged excitations. *Phys. Rev. Lett.*, 50:1395–1398, May 1983.

[61] G. Fano, F. Ortolani, and E. Colombo. Configuration-interaction calculations on the fractional quantum Hall effect. *Phys. Rev. B*, 34:2670–2680, Aug 1986.

[62] B. I. Halperin. Theory of the quantized Hall conductance. *Helv. Phys. Acta*, 56:75–102, 1983.

[63] Anthony Tylan-Tyler and Yuli Lyanda-Geller. Phase diagram and edge states of the $\nu = 5/2$ fractional quantum hall state with landau level mixing and finite well thickness. *Phys. Rev. B*, 91:205404, May 2015.

[64] Anthony Tylan-Tyler and Yuli Lyanda-Geller. In-plane electric fields and the $\nu = \frac{5}{2}$ fractional quantum hall effect in a disk geometry. *Phys. Rev. B*, 95:121302, Mar 2017.

[65] F. D. M. Haldane and E. H. Rezayi. Periodic Laughlin-Jastrow wave functions for the fractional quantized Hall effect. *Phys. Rev. B*, 31:2529–2531, Feb 1985.

[66] E. H. Rezayi and F. D. M. Haldane. Laughlin state on stretched and squeezed cylinders and edge excitations in the quantum hall effect. *Phys. Rev. B*, 50:17199–17207, Dec 1994.

[67] George Simion and Yuli Lyanda-Geller. Non-Abelian $\nu = \frac{1}{2}$ quantum hall state in Γ_8 valence band hole liquid. *Phys. Rev. B*, 95:161111, Apr 2017.

[68] Paul Soulé and Thierry Jolicoeur. Edge properties of principal fractional quantum hall states in the cylinder geometry. *Phys. Rev. B*, 86:115214, Sep 2012.

[69] X. G. Wen and A. Zee. Shift and spin vector: New topological quantum numbers for the Hall fluids. *Phys. Rev. Lett.*, 69:953–956, Aug 1992.

[70] *NIST Digital Library of Mathematical Functions*. http://dlmf.nist.gov/, Release 1.0.18 of 2018-03-27. F. W. J. Olver, A. B. Olde Daalhuis, D. W. Lozier, B. I. Schneider, R. F. Boisvert, C. W. Clark, B. R. Miller and B. V. Saunders, eds.

[71] I. S. Gradshteyn and I. M. Ryzhik. *Table of integrals, series, and products*. Elsevier/Academic Press, Amsterdam, 8th edition, 1965.

[72] Sonika Johri, Z Papić, P Schmitteckert, R N Bhatt, and F D M Haldane. Probing the geometry of the Laughlin state. *New Journal of Physics*, 18(2):025011, 2016.

[73] A. G. Moghaddam, T. Kernreiter, M. Governale, and U. Zülicke. Exporting superconductivity across the gap: Proximity effect for semiconductor valence-band states due to contact with a simple-metal superconductor. *Phys. Rev. B*, 89:184507, May 2014.

[74] P G de Gennes. *Superconductivity of Metals and Alloys*. Addison-Wesley Publishing Company, 1966.

[75] Michael Tinkham. *Introduction to Superconductivity*. Dover Publications, Mineola, N.Y., 2nd edition, 2004.

[76] Gabriele Giuliani and Giovanni Vignale. *Quantum Theory of the Electron Liquid*. Cambridge University Press, 2005.

[77] Matthew P. A. Fisher. Cooper-pair tunneling into a quantum hall fluid. *Phys. Rev. B*, 49:14550–14553, May 1994.

[78] A. Yu. Zyuzin. Superconductor–normal-metal–superconductor junction in a strong magnetic field. *Phys. Rev. B*, 50:323–329, Jul 1994.

[79] Cécile Repellin, Ashley M. Cook, Titus Neupert, and Nicolas Regnault. Numerical investigation of gapped edge states in fractional quantum Hall-superconductor heterostructures. *npj Quantum Materials*, 3(1):14, 2018.

[80] Maissam Barkeshli, Chao-Ming Jian, and Xiao-Liang Qi. Twist defects and projective non-Abelian braiding statistics. *Phys. Rev. B*, 87:045130, Jan 2013.

[81] Maissam Barkeshli and Xiao-Liang Qi. Synthetic topological qubits in conventional bilayer quantum Hall systems. *Phys. Rev. X*, 4:041035, Nov 2014.

[82] Yuli Lyanda-Geller. Topological transitions in Berry's phase interference effects. *Phys. Rev. Lett.*, 71:657–661, Aug 1993.